# How to trace the origins of short-lived atmospheric species: an Arctic example

Anderson Da Silva[1], Louis Marelle[1], Jean-Christophe Raut[1], Yvette Gramlich[2], Karolina Siegel[3,4], Sophie L. Haslett[3,4], Claudia Mohr[2,6], and Jennie L. Thomas[5]

[1]Laboratoire ATMosphères, Observations Spatiales (LATMOS), Sorbonne Université, UVSQ, CNRS, Paris, France
[2] Center for Energy and Environmental Sciences, Paul Scherrer Institute, Villigen PSI, Switzerland
[3]Department of Environmental Science, Stockholm University, Stockholm, Sweden
[4]Bolin Centre for Climate Research, Stockholm University, Stockholm, Sweden
[5]Université Grenoble Alpes, CNRS, INRAE, IRD, Grenoble INP, IGE, Grenoble, France
[6]Department of Environmental Systems Science, ETH Zurich, 8092 Zürich

**Correspondence:** Anderson Da Silva (anderson.da-silva@latmos.ipsl.fr)

The origins of particles and trace gases involved in the rapidly changing polar climates remain unclear, limiting the reliability of climate models. This is especially true for particles involved in aerosol-cloud interactions with polar clouds. As detailed chemical fingerprinting measurements are difficult and expensive in polar regions, backward modeling is often used to identify the sources of observed atmospheric compounds. However, the accuracy of these methods is not well quantified. This study provides an evaluation of these analysis protocols, by combining backward trajectories from the FLEXible PARTicle dispersion model (FLEXPART) with simulations of tracers from the Weather Research and Forecast model including chemistry (WRF-Chem). Knowing the exact modeled tracer emission sources in WRF-Chem enables a precise quantification of the source detection accuracy. The results show that direct interpretation of backward model outputs, or more advanced analysis like potential source contribution functions (PSCFs) are often unreliable in identifying emissions sources. After exploring parameter sensitivities thanks to our simulation framework, we present an updated and rigorously evaluated backward modeling analysis protocol for tracing the origins of atmospheric species from measurement data. Two tests of the improved protocol on actual aerosol data from Arctic campaigns demonstrate its ability to correctly identify known sources of methane sulfonic acid and black carbon. Our results reveal that traditional backtrajectory methods often misidentify emission source regions. Therefore, we recommend using the method described in this study for future efforts to trace the origins of measured atmospheric species.

## 1 Introduction

The warming rate of the Arctic is almost four times higher than the global average rate (Rantanen, 2022). In the austral hemisphere, the Antarctic ice sheet raises concern while its melting accelerates (Bronselaer et al., 2018). This polar amplified warming is concerning for the entire climate sciences community due to its possible impacts on the atmospheric and ocean circulations (Serreze and Barry, 2011). Studying the rapidly changing polar climates is therefore a research priority.

Short-lived climate forcers, such as aerosols and ozone, play an important role for global and polar climates (IPCC, 2021). Polar regions are especially sensitive to local forcing (Stuecker et al., 2018), and understanding the origin of short-lived climate forcers in these regions is especially important. Their climate impact is dominated by aerosol-cloud interactions, the effect of aerosols on cloud formation and evolution (Storelvmo, 2017). However, our understanding of aerosol forcing remains especially uncertain because of the complexity of their processes and the scarcity of measurements in the polar regions. Polar clouds could be more sensitive to aerosols than in other regions, because clouds are usually more sensitive to aerosols in clean conditions (Carslaw et al., 2013). In addition, aerosol-cloud interactions are even more uncertain in ice-containing clouds, which are predominant in polar regions (Matus and L'Ecuyer, 2017).

Controversies remain in the scientific community on the nature and sources of the atmospheric species implicated in these mechanisms. For instance, origins of particles acting as cloud condensation nuclei (CCN, necessary for liquid cloud droplet formation) or ice nucleating particles (INPs, involved in cloud ice formation) are sources of great debate (e.g., Zhao et al., 2024). Because modeling of CCN and INP species is often imprecise or even lacking in climate models (Morrison et al., 2020), an improved knowledge of their sources would help to fill the present gaps (Murray et al., 2021). In this context, being able to identify the sources of aerosols relevant for CCN and INP would be decisive in order to improve our understanding of their emissions, how to represent them in models, and how to quantify their impacts on polar clouds and climate.

In order to identify the origin of observed species, observational studies often rely on analyzing their detailed chemical composition and physical properties (Freitas et al., 2022; Heutte et al., 2025; Parshintsev and Hyötyläinen, 2015; Shao et al., 2022), or their correlation with chemical tracers like carbon monoxide from biomass burning and fossil fuel combustion (Jiang et al., 2009), or dimethyl sulfide from phytoplankton blooms (Park et al., 2017). These extra measurements are often expensive and not systemically present in measurement campaigns, and their interpretation is hardly straightforward.

Another way to identify the sources of observed species is to use backward modeling, in an attempt to track their atmospheric path all the way back to the emission sources. This does not require extra experimental data and has the advantage of costing less than observational methods. For example, this kind of analysis is increasingly used and presented alongside the analysis of INP observations. Some studies use straightforward interpretation of single backtrajectories (Allen et al., 2021; Hartmann et al., 2020, 2021; Porter et al., 2022; Wex et al., 2019; Yun et al., 2022), while others performed more advanced analysis like potential source contribution functions (PSCFs) (Irish et al., 2019; Si et al., 2019). Even though the methods used vary from a study to another, the conclusions about the possible emission sources can be interpreted similarly among the community, which could be misleading.

Backward modeling consists in the computation of particles path back in time within a fluid. As Chemistry Transport Models (CTM) give information on the future path of particles or chemical species, a backtrajectory model helps to trace back the fluid parcels that contain the species of interest. For atmospheric studies, many models offer solutions for backtrajectory computation. Among the most used we find two types of approaches. First, trajectory models using solely the resolved wind fields without turbulence or convection parameterization, like HYbrid Single-Particle Lagrangian Integrated Trajectory (HYSPLIT) (Stein et al., 2015), LAGRANTO (Sprenger and Wernli, 2015). Second, the Lagrangian particle dispersion models (LDPMs) like FLEXPART (Pisso et al., 2019), NAME III (Jones et al., 2007), or the Stochastic Time-Inverted Lagrangian Transport model (STILT) (Wen et al., 2012). One should know that HYSPLIT can also be run in dispersion mode. In the following, we will refer to the outputs of the first model category as *backtrajectories*, and to dispersion model outputs as *potential emission sensitivity* (PES). Both model types will be referred to as Lagrangian models.

Four different approaches that use Lagrangian modeling can be cited: 1) inverse modeling methods, 2) ratio methods or potential source contribution function (PSCF), 3) concentration-weighted trajectory (CWT) methods, and 4) direct interpretation of single backtrajectories or LPDM outputs. Inverse modeling (1) methods have been intensively used and developed since the 2000s, particularly for the retrieval of greenhouse gases emissions (Stohl et al., 2009; Manning et al., 2011; Brunner et al., 2012; Fang et al., 2015). They are more rarely applied to aerosol emissions source identification because of the challenge their high temporal and spatial variability represent (Dubovik et al., 2008; Partridge et al., 2011). Furthermore, these methods generally rely on a priori inputs on the emissions, such as satellite observations or existing but imprecise emission inventories. PSCF (2) (Ashbaugh et al., 1985; Zeng and Hopke, 1989) and CWT (3) (Hsu et al., 2003) are statistical methods that rely entirely on backward modeling and measurement time series. Because they are both easy to set up, they are intensively used (Polissar et al., 1999; Hirdman et al., 2010; Irish et al., 2019; Ren et al., 2021, e.g.). Nevertheless, interpretation of raw backtrajectories (4) is still common in the literature (references of INP studies herein above), and can lead to spurious conclusions about emission sources.

Fang et al. (2018) evaluated the performances of inverse modeling against CWT's and PSCF's, and concluded that the high quantitative power of inverse modeling surpasses the qualitative results of CWT and PSCF. Yet, PSCF and CWT are computationally low cost and can give useful insights when correctly applied and interpreted. The direct interpretation of backtrajectories remains the less reliable approach.

The present study focuses on the evaluation of low computational cost methods with little to no a priori knowledge on emission sources. The atmospheric species studied here are short-lived atmospheric compounds, such as aerosol particles, whose global observations are particularly challenging. To do so, we introduce a methodology based on simulated observations in a regional model that would allow the performances evaluation of any backtrajectory source identification methods. Here, we specifically test the widely used PSCF source identification method in order to assess its ability to qualitatively retrieve known sources of simulated emissions in the regional *Weather Research and Forecasting model including Chemistry* (WRF-Chem) model (Sec. 2.1.2). We use this approach to evaluate the PSCF method as used in Hirdman et al. (2010); Irish et al. (2019); Si et al. (2019) with the FLEXible PARTicle dispersion (FLEXPART) model (Sect. 2.3). Then, we propose three modifications to the PSCF method in order to improve its performance (Sect. 3). The method's sensitivities to its parameters are evaluated and thereby, the prerequisites for its application are identified (Sect. 4). Finally, a comprehensive example of the application to real-world observations of marine-sourced and land-sourced Arctic species are presented (Sect. 5), in order to demonstrate the improved method's performance on real cases.

## 2 Methods

The identification of atmospheric compounds emission sources with PSCF has been used for INPs (Irish et al., 2019; Si et al., 2019), atmospheric mercury (Hirdman et al., 2009), tropospheric ozone, black carbon (Hirdman et al., 2010), and more.

Previous studies only verified that the identified emission zones corresponded to expected areas. As it is commonly used, the method is only able to confirm expected emission sources. Identifying unknown sources necessitates a further assessed method. In this section we describe the models and methods we used to lead our study. The results are presented in Sect. 3.

### 2.1 WRF-Chem model for simulating concentration time series

In order to construct series of simulated concentrations at Arctic measurement sites with known emissions sources, we use the *Weather Research and Forecasting model including Chemistry* (WRF-Chem) regional model.

#### 2.1.1 Model setup

The WRF-Chem model is a widely used non-hydrostatic numerical model of mesoscale meteorology and atmospheric chemistry (Skamarock et al., 2022; Grell et al., 2005). The version used here is optimized for high latitudes and presented in detail in Lapere et al. (2024) and Marelle et al. (2017).

WRF-Chem is guided by Final Operational Global Analysis data (FNL) from the American *National Center for Environmental Prediction*, with six hours time-steps. The simulation is run on a $10,000\ \mathrm{km} \times 10,000\ \mathrm{km}$ square domain centered on the north pole, with an horizontal resolution of $50\ \mathrm{km}$ and 72 vertical levels. The WRF version used for this study is 4.3.1. The detail of the options used for the simulations are described in Table A.

#### 2.1.2 Tracer emission

The WRF-Chem model is used to simulate the emissions, transport and removal of three different tracers on a duration of 24 months (September 2019 to September 2021). The latter are short-lived particles with wind-dependent emissions. Each of them represents the emissions of surface type sources categorized as follow: continental, oceanic from ice-free regions, and oceanic from sea ice regions. The continental tracer corresponds to mineral dust or continental biogenic aerosols, the open ocean tracer represents sea spray emissions, and the sea ice tracer is associated with blowing snow emissions. We chose to focus on natural sources because they are not well constrained in the Arctic. In addition, their relative contributions to the emissions of CCN and INPs is still unclear (Burrows et al., 2013; Gong et al., 2023; Hartmann et al., 2021), which motivates us to study those types of particles. Nevertheless, the results of this experiment stay valid for other atmospheric species.

The emissions are led by processes relying on wind speed with surface type dependency. The detailed definitions are presented in Table 1. Because of the long duration of the modeling experiment, the tracers would accumulate infinitely in the domain without removal. In order to keep the study as general as possible, we decided not to set advanced removal processes, namely dry and wet removal, since those highly depend on the nature of the studied species. This is the case for aerosol particles, whose removal strongly depends on their size and hygroscopy (Ohata et al., 2016; Farmer et al., 2021). Since the study focuses on short-lived species, the tracers are removed thanks to an exponential decay with a characteristic time of three days. This allows the exact same removal in both WRF-Chem forward and FLEXPART-WRF backward simulations, thus the

**Table 1.** Tracer parameters in WRF-Chem-Polar.

| Tracer name | Regional condition | Parameterization |
|---|---|---|
| Sea ice | Over ocean, with sea ice fraction larger than 0.5 | Monahan et al. (1986) |
| Open ocean | Over ocean, with sea ice fraction smaller than 0.5 | Monahan et al. (1986) |
| Continent | Over continental regions | Ginoux et al. (2001) |

The parameterizations refer to the application of the condition on wind speed.

evaluation is free of the uncertainties on removal parameterizations. In that way, the evaluation setup is idealized, and accounts only for the best performances that can be expected from the tested methods.

#### 2.1.3 Tracer interpolation at Arctic sites

The concentrations of each tracer are daily interpolated at the coordinates of five Arctic stations: Alert (Canada), Ny-Ålesund (Svalbard), Tiksi (Russia), Utqiaġvik (Alaska) and Villum (Greenland). Series of simulated concentrations of the three tracers can therefore be set up. The five stations were chosen for their distribution around the Arctic basin (Fig. 1e). This distribution sets the conditions for assessing the spatial sensitivity of the method in this region. Furthermore, many measurement campaigns are conducted at these stations (e.g. the Ny-Ålesund Aerosol Cloud Experiment, NASCENT (Pasquier et al., 2022)).

Figure 1 presents the emission regions (panels a, b, c) of the three tracers through their integrated emissions over one year of simulation. Panel (d) shows an example of a reconstructed series of concentrations interpolated at the coordinates of the Svalbard station, Ny-Ålesund. A seasonal variability of the concentrations can be clearly detected, which is in accordance with actual observations of Arctic species. This variability is mainly due to seasonal variations of mesoscale atmospheric transport and to local wind speeds (both phenomenons reproduced by WRF). Nevertheless, not all simulated concentration series show such a variability, it depends of the tracer and the station. The strongest variability is found for the continental tracer; the lowest for the sea ice one. More broadly, the farther the emission source from the station, the weaker the observed variability.

Reproducing real concentrations series is not in the scope of this study. Therefore, even though the tracers have aerosol particles like properties, the interpolation of their concentrations does not mimic instrumentation used for this type of measurement. Consequently, it is important to note that these series can not be assimilated to actual concentrations of any atmospheric species.

The knowledge of the tracers emissions conditions peculiar to this experiment allows the evaluation of the method performances. Theoretically, a perfectly working method of tracking would point out the exact sources of emission that correspond to each tracer. Practically, the performances of backward methods are heterogeneous among tracers and from a station to another. Section 3.3 discusses the way the method should be applied in order to get the best performances and what parameters drive its success.

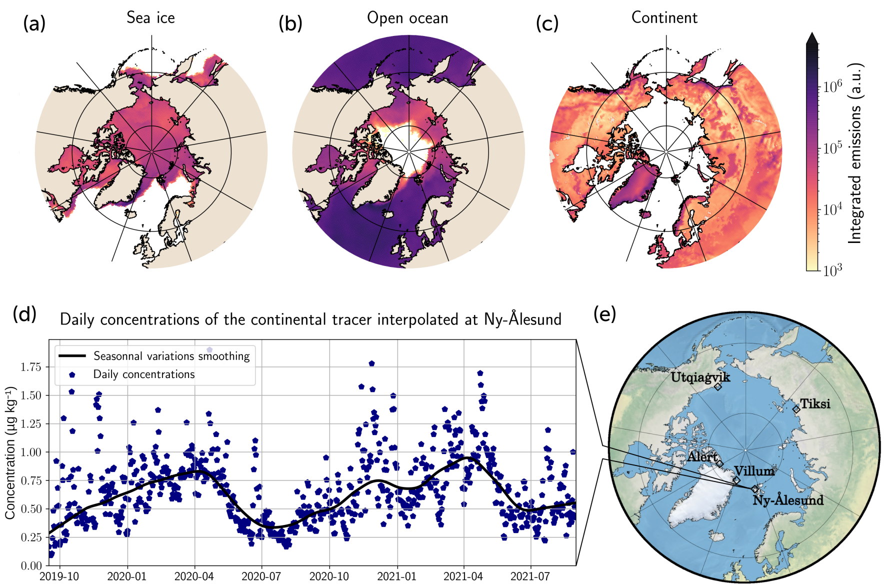


**Figure 1.** Overview of the tracers emissions in WRF-Chem and concentration series reconstructions. Regions of emissions of sea ice (a), open ocean (b) and continental (c) tracers. (d) Example of reconstructed series of daily concentrations interpolated at Ny-Ålesund. (e) Map of the Arctic with the locations of the five studied stations. Base map from Cartopy © British Crown copyright, 2016

### 2.2 PES plumes with FLEXPART-WRF

FLEXPART belongs to the family of Lagrangian Particle Dispersion Models (LPDMs). These are stochastic tools for the modeling of large amount of air tracers. The Lagrangian approach allows for reduced numerical diffusion (Cassiani et al., 2016) which therefore leads to better capturing atmospheric diffusion than Eulerian models (Pisso et al., 2019). LPDMs also show the advantage of remaining independent of the model grid resolution since they use Lagrangian approach. This accounts for the recommended utilisation of LPDMs for the interpretation of PES in sources tracing (Stohl et al., 2002).

FLEXPART (Pisso et al., 2019) simulates emission, diffusion, and deposition processes (wet and dry) or time-based decay of atmospheric tracers. The emission is done through single or multiple volume sources, and the simulation can be run forward or backward in time. The path of the emitted tracers is followed through a plume representation expressed in terms of PES in seconds. It can be likened to the resident time of particles in each grid cell. This information surpasses the direction of origin commonly given by simple trajectories (Hirdman et al., 2009). The FLEXPART performances have been validated with multiple atmospheric tracers release experiments (Stohl et al., 1998). Furthermore, Hegarty et al. (2013) demonstrated the FLEXPART ability for reconstructing dispersion of atmospheric tracers.

When investigating ground emissions, it is common to introduce the footprint PES (FPES), defined as the PES of the first FLEXPART vertical level. The latter will be defined here as the first $100\ \mathrm{m}$ above ground level. Here we use the FLEXPART-WRF version of the model. It is optimized to use WRF output data (cf. Sect. 2.1), allowing the control of meteorological variables through WRF. In FLEXPART-WRF, several FLEXPART schemes are replaced by the WRF's ones (Brioude et al., 2013). It intends to give information on the particles origins. The accuracy of the transport patterns simulated by FLEXPART-WRF decreases with the augmentation of the backward simulation duration and relies on the accuracy of the initial WRF simulation in terms of meteorological variables.

#### 2.2.1 Emission configuration in FLEXPART

The tracers in FLEXPART are characterized with five parameters (Table 2). First, we define the release time of the particles. In our case, the model emits on a whole day corresponding to the associated in situ measurement (Sect. 2.1.2). Then, we set the release box, which is defined as a $50\ \mathrm{km}$-wide and $10\ \mathrm{m}$ high box. The trajectories are computed backward in time for seven days before the time of release. An amount of $100,000$ particles is released in the emission box. The sensitivity of the PES plume to the number of released particles is inversely proportional to this number. Although this sensitivity is low, a rate of $10,000$ particles emitted per hour is recommended. Finally, we can set different schemes for the tracers' dry and wet deposition. For the experiment depicted in Sect. 2.1.2 we set an exponential decay similar to the WRF-Chem tracers used to construct the concentration time series.

**Table 2.** Emission parameters for FLEXPART-WRF.

| **Parameter** | **Description** |
|---|---|
| Release period | Day of measurement (1 day) |
| Release box | $50 \times 50$ km-wide and $10\ \mathrm{m}$ tall box covering the measurement site |
| Backward duration | 7 days |
| Number of released particles | $100,000$ |
| Deposition | Exponential decay with $\tau = 3$ days* |

* Deposition parameters can be set differently depending on the studied species.

The complete FLEXPART-WRF configuration file used here is available (cf. Data and Code availability). FLEXPART-WRF is run for every day of the synthetic concentration series (715 days at the 5 different locations) with the parameters described hereinabove. Finally, the ratio method (Sect. 2.3) is applied on the FLEXPART-WRF outputs, and the results are analysed for the three tracers (sea ice, open ocean, continent) independently.

### 2.3 Statistical source identification method

In this study, we work on a statistical analysis method of backtrajectories or PES, that relies on the computation of PSCFs. The method is itself inspired by the analysis protocol introduced by Ashbaugh (1983) and Ashbaugh et al. (1985). Since then, backward models evolved significantly, and the method was used in many studies about sources of atmospheric species (Sect. 1). In the following, we will stick to the PSCF methodology introduced in Hirdman et al. (2010) without the bootstrapping post analysis, like it is mostly applied in the studies that use it. It will be referred to as the "ratio method".

The approach relies on both atmospheric species concentrations measurements and model outputs from FLEXPART-WRF. For each point of the concentration series, a FLEXPART-WRF simulation is run in backward mode. Then, the outputs of every run are sorted according to the measured particles concentration they are associated with. The great majority of earlier studies relying on backward analysis stop here without further analysis. Notwithstanding at this step, we only have information on the direction of origin, with proximity bias near the measurement site. In the present study, we use a deeper analysis described as follows.

Let us consider $S_\mathrm{t}$ as the average of the FPES fields from a set of $N$ FLEXPART-WRF runs:

$$S_\mathrm{t} = \frac{1}{N}\sum_{n=1}^{N} S(n) \tag{1}$$

where $N$ is the number of model runs, and $S(n)$ the array of FPES associated with the measurement $n$.

$S_\mathrm{t}$ can be interpreted as the climatology of the origins of air masses that are associated with the particle concentrations series on the studied period. We can sort the concentrations in order to select the $P = \frac{x \times N}{100}$ highest and lowest concentrations, with $x$ the percentage of selection. Thus, if $S$ is the series of FPES fields sorted from the lowest to the highest measurement value, we can define $S_\mathrm{h}^x$ and $S_\mathrm{l}^x$ the climatologies of the origins of air masses associated with respectively the $P$ highest and lowest particle concentrations. These new fields are expressed as follows,

$$S_\mathrm{h}^x = \frac{1}{P}\sum_{n=N-P}^{N} S(n) \tag{2}$$

$$S_\mathrm{l}^x = \frac{1}{P}\sum_{n=1}^{P} S(n) \tag{3}$$

As the PES decrease with distance from the measurement site, a proximity bias is observed on these climatologies, giving the impression of mainly local sources. To eliminate that bias, we compute the ratio of $S_\mathrm{h}^x$ (respectively $S_\mathrm{l}^x$) to the total climatology $S_\mathrm{t}$. We thus can define $R_\mathrm{h}^x$ and $R_\mathrm{l}^x$, the respective ratios of the "high" and "low" climatologies,

$$R_\mathrm{h}^x = \frac{P}{N}\frac{S_\mathrm{h}^x}{S_\mathrm{t}} \tag{4}$$

$$R_\mathrm{l}^x = \frac{P}{N}\frac{S_\mathrm{l}^x}{S_\mathrm{t}} \tag{5}$$

Values equal to $f = x/100$ indicate no deviation from the average field $S_\mathrm{t}$. Consequently, the points where $R_\mathrm{h}^x$ is higher than $f$ correspond to regions of likely origins for the studied particles. The same reasoning applied on $R_\mathrm{l}^x$, leads to the conclusion that the corresponding field indicates no longer the presence but the absence of sources or even the presence of sinks.

One should be aware that the significance of $R_\mathrm{h}^x$ and $R_\mathrm{l}^x$ is proportional to the value of $S_\mathrm{t}$. Low values of $S_\mathrm{t}$ indicate few transport through the corresponding grid points and therefore can invalidate the statistical results of the ratios computation.

Practically, too high values of the ratio can be suspected as spurious indications. However, if the percentage $x$ is strict (i.e. low) enough or the total number N of runs is large enough, these excessively high values should not appear.

In the following, we will discuss furthermore how to define a threshold on FPES in order to prevent false interpretation of the ratio fields. Because the ratio method allows to eliminate the FLEXPART proximity bias, it can miss the detection of very local sources when applied on a large domain. However, this effect being only proportional to the domain size and resolution, it can be mitigated by either increasing resolution or downscaling the domain.

## 3 Results

### 3.1 Metric of evaluation

The main result of the ratio method is the ratio map associated with the highest concentrations of the studied series. By itself, it gives qualitative information on the sources origin of the species. In order to get some quantification, we use the definition of the surface types that corresponds to the tracers emission (Table 1). Masking the ratio maps with continental, open ocean and sea ice masks and then summing the ratio values corresponding to these surface types, we get a quantification of the actual detection performed by the method. We introduce the detection score $D_T$, define as follows:

$$D_T = \frac{R_T}{R} \tag{6}$$

where $D_T$ refers to the signal contribution of the surface type corresponding to the tracer $T$ (sea ice, open ocean, continent), $R$ is the result signal ($R_{\mathrm{h}}^{10}$ in the standard method or $R_{\text{10-33}}$ in the improved method, c.f. Sect. 3.3), and $R_T$ is the sum of $R$ over the surface type corresponding to the tracer $T$. A perfect detection would be a full contribution of the surface type that corresponds to the analysed tracer, i.e. $D_T = 1$. For instance, the method applied on the concentrations of the continental tracer should lead to a detection of the continent, with a limited contribution of sea ice and open ocean regions. In that case, $D_T$ would tend towards 1. Practically, the ratio method gives various results. Therefore, a metric with five levels of success has been defined to catch the fluctuations of the method performances. Table 3 describes the metric levels. Good confidence is attributed to the results when level 2 is reached. Levels 0 and 1 call for special attention and map analysis.

**Table 3.** Definition of the criteria for the evaluation of the ratio method results.

| Level of success | Criteria |
|---|---|
| 0 | $D_T$ is not first contribution |
| 1 | $D_T$ is first contribution |
| 2 | $D_T > 0.5$ |
| 3 | $D_T > 0.5$ and second contribution $< 0.25$ |
| 4 | $D_T > 0.8$ |

## 3.2 The standard ratio method

In this section, we use the ratio method, or PSCF method, as presented in Sect. 2.3. We apply it on the simulated data constructed with the numerical experiment presented in section 2.1.2. For clarity, we present one case: retrieving the sources of continental tracer emissions from the Ny-Ålesund simulated concentration series.

Figure 2 illustrates the application of the ratio method on one of the tracers simulated in the idealized experiment (Sect. 2.1.2). The ratio maps for the three tracers and the five stations are available in the supplementary materials (Fig. S1). Panel (a) shows the concentration series of the continental tracer interpolated at Ny-Ålesund over two years of simulation. Highest and lowest concentrations are flagged with respectively red and cyan colors. The second line of Fig. 2 is dedicated to the maps of FPES (panels (b) and (c)) and to the ratio map (panel (d)). The map (b) corresponds to the $S_\mathrm{t}$ defined in Sect. 2.3. It is the climatology of the origins of all the air masses ending at Ny-Ålesund over the two years of simulation. Similarly, (c) shows $S_\mathrm{h}^{10}$, the climatology of the air masses origins that contained the 10% highest continental tracer concentrations of the series. Finally, (d) shows the ratio of $S_\mathrm{h}^{10}$ over $S_\mathrm{t}$ which has been presented as $R_\mathrm{h}^{10}$. This ratio map, or PSCF map, is the result map of the ratio method. It shows various regions of likely sources for the continental tracer time series. Greenland and Canada ahead, there is also less continuous signal spots in Eurasia. Even though there is some signal overflow over the north Pacific, the Baffin bay and a small amount over the Arctic ocean, the quantification metric (defined in Sect. 3.1) gives to this case a score of 2. It means that the continental source is correctly detected.

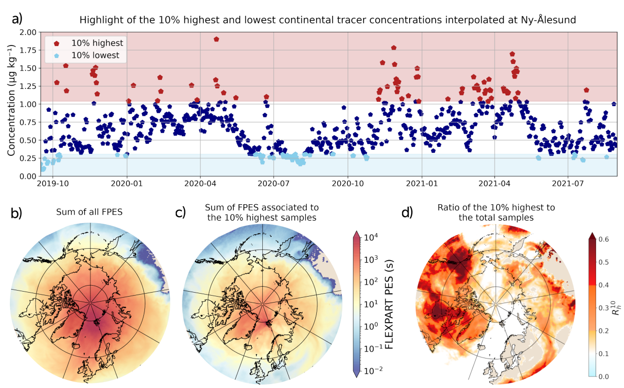


**Figure 2.** Application of the ratio method as it is depicted in Sect. 2.3. Panel (a) shows the reconstructed daily concentration series of the continental tracer interpolated at Ny-Ålesund on the two years of simulation. (b) is the climatology of the total air masses origins, (c) the climatology of the origins of air masses that brought the 10% highest concentrations, and (d) is the ratio of (c) on (b), noted $R_\mathrm{h}^{10}$.

The results for the continental tracer on the other stations (Alert, Tiksi, Utqiaġvik, excepted Villum) reach success (as it will be seen in Fig. 4a). Nevertheless, the application of the method on both sea ice and open ocean tracers gives poor results. Only Ny-Ålesund and Tiksi show a correct detection for the open ocean case. Otherwise, all the other detection fail, showing the continent as the main contributor (Fig. 4a). This observation questions the reliability of the continental tracer results. Indeed, a geographical bias strengthens the continental signal. We can identify three reasons for this behavior. Firstly, the domain of simulation tends to over represent continental regions. Indeed, the continent accounts for 53% of the total surface area, when the open ocean and the sea ice regions represent on average 37% and 10% respectively. In the idealized situation of exact back-tracking of the air masses, this bias should not affect the detection results. However, dispersion modeling is innately imperfect. The computation of the ratio induces loss of information on FPES intensity. The latter is replaced by the ratio values which can reach its saturation value of one for regions where very few FPES plumes passed. If an area is covered only by FPES plumes associated with the highest concentrations of the measurement series, we get a saturation of the ratio. Thereby, regions of very low FPES can end up highlighted on the ratio map even though they are not statistically significant values. Consequently, irrelevant signals affect the detection, likely benefiting the predominant surface type, namely the continent in this Arctic situation. Secondly, and to a lesser extent, the other reason for biased results is the seasonal variability of the concentration series. As described in Sect. 2.1.2, the simulated concentrations vary during the year, with maximum concentrations in winter/spring and low concentrations in summer and autumn, following the well known Arctic Haze seasonal cycle. The latter is due to efficient transport of air masses from land masses in the mid-latitudes during spring (Schmale et al., 2022). As a result, applying the ratio method on annual observations of short-lived pollutants in the Arctic produces a climatology of air mass origins in winter and spring, and is biased for lower latitude sources, over-representing continental sources as seen in our evaluation on Fig. 4a. Last but not least, any source attribution method based on a single observing site will suffer from a so-called “shadowing” effect. This tends to falsely assign emissions to areas that are upwind of the true emitting area. In the present case and for the sea ice and ocean tracer, the continental areas are mostly in such a configuration. The only way to robustly overcome this problem, is a network of sites that can observe gradients across the domain, or at least "observe" the same source area under different flow directions (as demonstrated in Sect. 3.5). These implications suggest that the ratio method, as applied in the section, is not suitable for studies involving real measurement data.

The next section will present and discuss the improvements that make the method reliable for real case studies.

### 3.3 Improving the ratio method

In Sect. 3.2, the standard ratio method gave ambiguous results. In this section, we present how one can improve the method in order to get more reliable source identification.

To eliminate the seasonal variability bias, we sort the concentrations upon their differences to the seasonal trend of the series, rather than sorting them with their absolute values. Practically, we estimate the seasonal trend by fitting the series and then subtracting it from the concentrations. This is similar to the background subtraction methods of Ruckstuhl et al. (2012) and Resovsky et al. (2021). Practically, we estimated the background seasonal concentration by smoothing the series with a locally weighted scatter plot smoothing (LOWESS) filter, and then subtracting the background trend from the concentrations to keep the high frequency signal from recently added emission events.

Concerning the over representation of the continental area, a cutting threshold on FPES is set in order to filter the less significant FPES. This is similar to the approach of Fang et al. (2018), who suggested excluding grid cells crossed by too few trajectories. The values of $S_\mathrm{t}$, $S_\mathrm{h}$ and $S_\mathrm{l}$ under this threshold are removed for the ratio computation. The risk with this tuning is to loose information while filtering the lowest FPES values. We performed tests in order to identify the best threshold, using the idealized tracers experiment for the assessment. The details of the latter are discussed in Sect. 4. Best results are obtained for a variable threshold that filters out the 2 % lowest FPES of the studied case. The threshold varies from a case to another in order to always remove the 2 % lowest FPES values. It is worth noting that applying a filter on FPES or PES values is on average equivalent to setting a threshold on the number of trajectories passing through a grid cell. In this manner, we remove the majority of FPES which are less statistically significant.

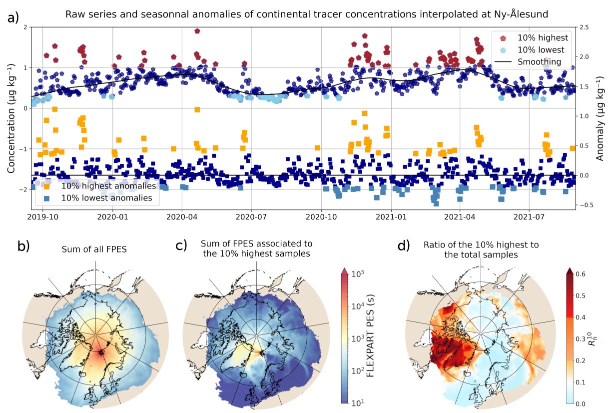


**Figure 3.** Application of the improved ration method. Similarly to Fig. 2, (a) shows the reconstructed daily concentration series of the continental tracer interpolated at Ny-Ålesund with the comparison of the standard sorting (top) and the seasonal sorting (bottom). (b) is the climatology of the total air masses origins, (c) the climatology of the origins of air masses that brought the 10 % highest concentrations, and (d) is the ratio of (c) on (b), noted $R_{\mathrm{h}}^{10}$. In (b) and (c) the 2 % lowest FPES have been removed, as explained in Sect. 3.3.

These two modifications to the ratio method are illustrated in Fig. 3. Panel (a) displays the original concentration series with the classical sorting of high and low values (top), as well as the series constructed with the differences to the seasonal variations (bottom). The highest values of the latter are flagged in yellow. They are more evenly distributed along the simulation period than the raw concentrations. The effect is even clearer for the lowest concentrations; some of the lowest points happen in the cold season, which was never the case with the standard sorting method. Panels (b), (c) and (d) highlight the effect of the filtering threshold on FPES. Indeed, removing the 2 % lowest FPES erased a corona of values clearly visible on the climatology maps. The ratio map of panel (d) presents a much smaller area of values above 0.1. The overflows over sea ice and open ocean regions are greatly reduced. The Baffin Bay is the region where incorrect signal remains. This shows that shadowing can still happen, especially around regions of intense emissions. The north American and Eurasian signals decreased as well. Even though they correctly corresponded to continental emissions, their significance is considered as low because they were due to regions of low FPES. The quantification of the detection indicates a level of success for this case of 3, when the standard method only gave a value of 2.

In order to take maximum advantage of the ratio method, the information contained in the ratio associated with the lowest concentrations can also be used. Indeed, this ratio points the regions where the sources do not likely come from. Thus, its reverse $(1 - R_{\mathrm{l}})$ can be used as a mask applied on $R_{\mathrm{h}}$. We use $R_{\mathrm{h}} = R_{\mathrm{h}}^{10}$ and $R_{\mathrm{l}} = R_{\mathrm{l}}^{33}$. Thus we get a composite ratio defined as follows,

$$R_{\text{10-33}} = R_{\mathrm{h}}^{10} \times (1 - R_{\mathrm{l}}^{\uparrow 33}) \tag{7}$$

Where $R_{\mathrm{l}}^{\uparrow 33}$ are the values of $R_{\mathrm{l}}^{33}$ above 0.33. We choose to use $R_{l}^{33}$ rather than $R_{l}^{10}$ and $R_{l}^{5}$ because it considers more PES and thus it is a more statistically significant ratio. Additionally, unlike the ratio of high concentrations, we aim to select as many regions as possible that are detected as unlikely sources. To our knowledge, taking into account these areas of low concentrations in a PSCF method has not been tried in the past and is the most innovative part of our method. Testing the detection performances of the composite ratio showed improvement in six out of fifteen cases, and generally enhanced the number of correct attributions in 80 % of the cases. We therefore include the composite ratio as a final step for the improved ratio method.

The details of the performance improvements for each modification presented above, are given in Table 4 and discussed in the next section (Sect. 3.4).

### 3.4 Results comparison

The success levels allow easy comparison between the different ways the method is applied. Therefore, we can compare the performances of the standard method – as if we apply straight forward the ratio method described in Sect. 2.3 – with the results of the improved method presented above. Figure 4 illustrates these results.

As mentioned in Sect. 3.2, the assessment of the standard method (Fig. 4a) does not provide a level of confidence high enough to trust its results. The improved method performs better in ten out of fifteen tested cases (Fig. 4b), worse in one case, and equally otherwise, as reported in Table A2. As expected, the overall contribution of the continental source decreased thanks to the FPES filtering threshold. The open ocean suffered the same effect. The improved method detects much more accurately the origins of the open ocean, continental, and sea ice tracers, with correct attributions at 4/5 stations for the ocean tracer (3 in the original method), 3/5 for the ice tracer (0 in the original method), and 5/5 for the continental tracer (4 in the original). In addition, the quality of the detection score is improved or identical, degraded in only one case (open ocean tracer at Tiksi).The detection level averaged over the five stations and three tracers gives a general assessment of the methods. The standard ratio gets an averaged score of 0.9, which corresponds to a failed detection as defined in Sect. 3.1. The improved ratio method gets 2.0, which is where the threshold for good confidence in the results starts.

However, a few detection still fail. Figure S2 shows the composite ratio maps of the improved ratio method for all the stations and the three tracers. It enables the detailed examination of the identification results. The source detection of the sea ice tracer at Alert is highly polluted by continental signal. The composite ratio maps of this case give insight on the reason for this fail, presenting an overflowing shadowing of the plume on the continental regions (c.f. Sect. 3.2). The poor detection of the open ocean tracer at Alert and Utqiaġvik are due to hard shortening of the FPES from the threshold filtering. The plume mainly covers the regions of marginal sea ice. We observe the same thing for Tiksi, even though the map clearly shows the influence of

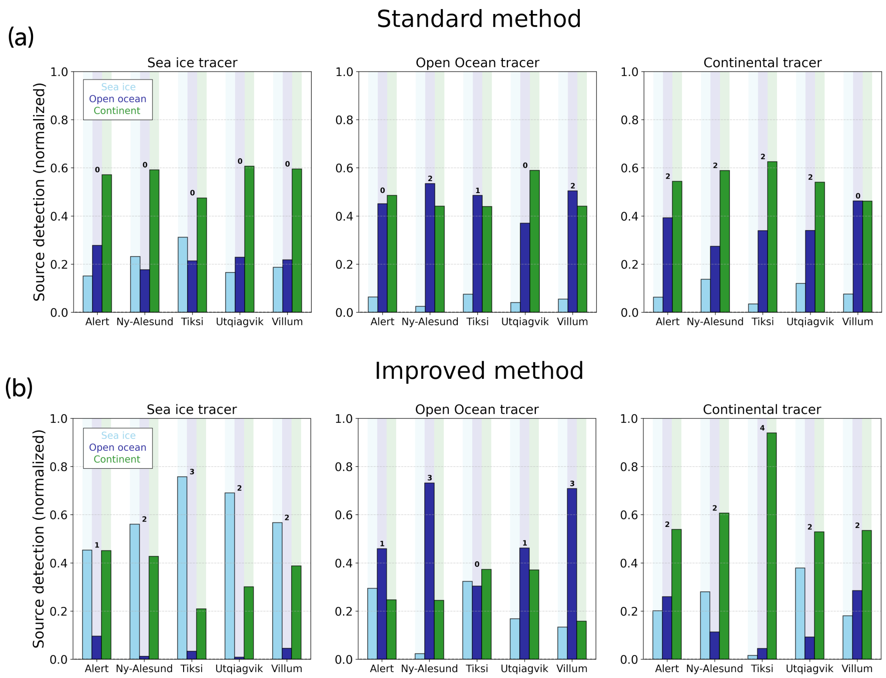


**Figure 4.** Comparison of the results obtained with the standard ratio method (a) and with the improved ratio method (b). Every panel presents the detection results for a specific tracer and for the five stations. The bars represent the contributions of each surface type to the detection (light blue for sea ice, blue for open ocean, green for continent). For every pair of tracer and station, the level of success is showed above the corresponding bars.

both north Pacific and north Atlantic. Anyway, and for all cases, the composite ratio maps give great information on the region of origin.

In order to assess the contributions of the three modifications (FPES filter, background subtraction, composite ratio) to the standard ratio introduced with the improved ratio, the sources identification has been run in the standard ratio setup with one or two improved ratio's modifications. The results are presented in Table 4. Each cell value corresponds to the averaged success level when the column and row modifications are used. Thus, the diagonal values refer to the detection score when a single modification is used in addition to the standard ratio; the others, when both the row and column modifications are used. The highest improvement is due to the FPES filtering with an improvement of $0.4$ compared to the standard ratio. The composite ratio allows a $0.2$ rise, where the background subtraction leads to an improvement of only $0.1$. The best combination appears to be the composite ratio with the FPES filter, which improves the score of the standard method by $0.7$. The combination of the composite ratio and the background subtraction only account for a $0.2$ improvement. Even though the latter seems to be a small improvement, the full potential of the improved ratio method is only reached when the three modifications are used all together. In other words, the three modifications are needed to reach an averaged detection level of 2, which is the threshold of a confident successful detection (Sect. 3.1). The detailed performances of these tests (i.e. for the three tracers and five stations) are presented in the supplementary materials (Fig. S3).

**Table 4.** Comparison of the averaged success levels when adding the different modifications to the standard ratio. Each cell gives the averaged level of detection when the column and row modifications are added to the standard ratio methodology. The corresponding score of the standard ratio is 0.9, and 2.0 for the improved ratio.

| | FPES filter | Background subtraction | Composite ratio |
|---|---|---|---|
| FPES filter | 1.3 | 1.5 | 1.6 |
| Background subtraction | 1.5 | 1.0 | 1.1 |
| Composite ratio | 1.6 | 1.1 | 1.1 |

The values are rounded to the first two digits.

### 3.5 Combination of stations

Some observations of atmospheric species are made within a measurement network composed of multiple experimental sites (e.g. ICOS, WMO GAW, NOAA flask network, AGAGE). The observations can therefore be simultaneous and equally distributed in time. This tends to draw a snapshot of the state of the atmosphere regarding the studied species or variables. This can also be achieved with satellite data, from which it is possible to interpolate quasi simultaneous time series at many different locations around the globe.

We can envision that the species of interest we want to study are or will be part of an observational network, or that it is measured by satellite observation. Therefore, how would the tracing method presented here take advantage of this? In order to answer that question, we compute the method combining the FPES associated with the five Arctic stations previously described, as a way of triangulating the sources. Once again, we are in the presence of an idealized situation: the concentrations series are perfectly simultaneous and derived identically. True observational data might drift from these perfect conditions, however we believe this experiment can illustrate the potential of such an application of the method.

For the combination, we kept the sorting of high and low concentrations specific to each station. We did as well for the sorting of the corresponding FPES plumes. The gathering is done at the step of ratio construction. $S_\mathrm{h}$ and $S_\mathrm{l}$ are computed as the sum of the corresponding ratios of every station. In the same way, the total climatology of the FPES plumes, $S_\mathrm{t}$, is now the sum of the PES plumes of the five stations. The ratios $R_\mathrm{h}$ and $R_\mathrm{l}$ are then calculated with equations 4 and 5.

The results show a successful source origin detection (Fig. 5). The continental sources are detected with a success level of 3, when the sea ice and open ocean get a success level of 2. This lower score for the open ocean could be explained by the geographical arrangement of the stations: open ocean regions are not well surrounded by the Arctic stations. When Villum and Ny-Ålesund are exposed to north Atlantic sea sprays, Utqiaġvik is hardly reached by these emissions. Conversely, the north Atlantic stations do not get much signal from north Pacific emissions. More generally, sea ice and open ocean results are affected by some continental signal due to systematic coastal overflow. This effect leads to lower scores even though the

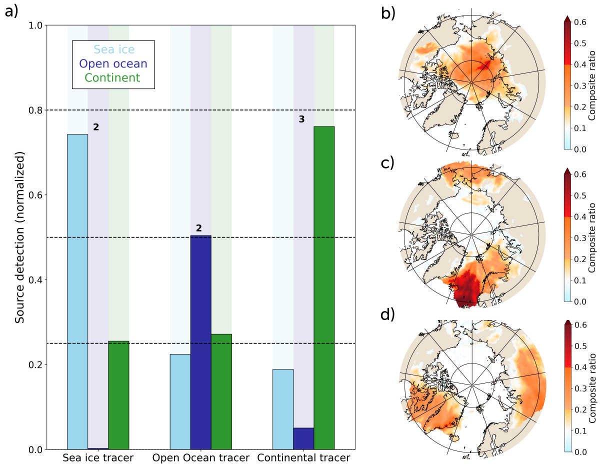


**Figure 5.** Results of the five stations combination. (a) shows the fraction of contribution of every surface type for the three tracers, and the associated success level. (b), (c) and (d) are the composites ratio maps for the sea ice tracer, the open ocean tracer and the continental tracer respectively.

composite ratio maps give clear insight on the origin regions. The existence of this unshrinkable surfeit of continental signal should be kept in mind when interpreting any results of similar application of the method.

Nevertheless, the combination of simultaneous observations of the same species has the potential to give precise clues on the regions of origins of the so-called species. The implementation of data from mid-latitude stations could also improve the results by increasing the spatial coverage. Therefore, the present work encourages the development of observational networks or coordinated field experiments dedicated to identify short-lived species at the high latitudes, following the example of the networks for greenhouse gas observations that are used to attribute global and regional emissions. The global deployment of the Portable Ice Nucleation Experiment (PINE) (Möhler et al., 2021) fits this recommendation for the study of INPs.

### 3.6 Points for using a ratio methodology

Eventually, we did not test the improved ratio method against raw FPES interpretation. In order to get an idea on how they compare, Fig. 6 shows, through the example of the sea ice tracer for the Tiksi station, different visualisations of the FLEXPART-WRF FPES. The first line shows the climatologies of the FPES over the period of observation. These representations are often used for quick qualitative source identification in studies using backtrajectories or PES (Fig. 6a and 6b). The second line shows the results of the ratio methods presented in this paper. What the figure reveals is that the sea ice origin of the tracer is only clearly found with the improved ratio method (6d and 6e). As a reminder, if the source detection was perfect, the light blue bar would reach one on Fig. 6e since the studied tracer was only emitted in sea ice regions. The climatologies, particularly Fig. 6b, provide general information about potential sources of the tracer. However, it does not allow for reliable quantification as seen in the corresponding column on Fig. 6e. Neither does the standard ratio method (6c), which gives – in this case – even worse

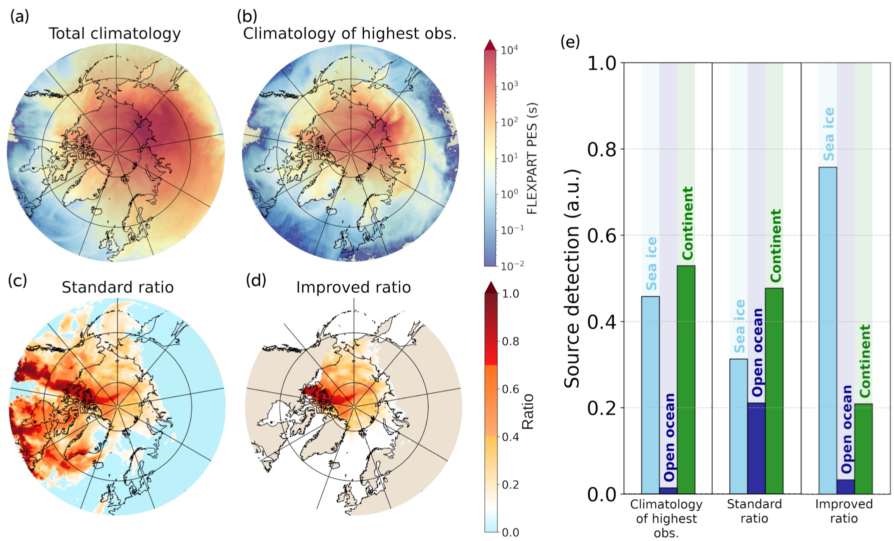


**Figure 6.** Panel of FPES visualisations and analysis for the sea ice tracer at the Tiksi station. (a) and (b) are the climatologies of respectively the total FPES and those associated with the 10 % highest observations ($S_\mathrm{h}^{10}$). (c) and (d) are the ratio maps of the two versions of the ratio method ($R_\mathrm{h}^{10}$ for respectively the standard and improved versions). (e) is the quantification of the detection results for the climatology associated with the highest observation and for both versions of the ratio method.

quantification results than the climatology. Let us mentioned that weighting the FPES plumes with the particles concentrations has also been tested, and did performed similarly as the climatology of the highest observed concentrations. Eventually, only the improved ratio method provides a clear map of the actual origins of the tracer (Fig. 6d compared to Fig. 1a) and enables unequivocal quantification of it.

## 4 Discussion on sensitivities

In this section, we investigate the sensitivity of our improved ratio method to key parameters: the sorting percentiles, the data series duration and frequency, and the filtering threshold on FPES.

### 4.1 Sorting percentiles

The standard ratio method uses the 10$^{\text{th}}$ percentile to sort the highest and lowest points of the measurements series. A higher threshold would address more points which can be needed for statistical representativeness when the series is short. Some studies use percentiles of 33$^{\text{rd}}$ or 36$^{\text{th}}$ percentile to define what are the highest measurements (Irish et al., 2019; Si et al., 2019). On such short series, selecting the highest third of measurement amounts to look at a few particular PES plumes, and the benefits of computing the ratio appears to be poor. On longer time series, using 33$^{\text{rd}}$ percentile to define the highest measurements casts too widely among the observations and makes the ratio unable to identify the sources of emissions. With such a high percentile, the method detects also some of the high concentration events due to particular atmospheric patterns, as well as some events of lower concentrations. This dims the source identification and makes it inefficient. Actually, the tests performed on the idealized tracers (Sect. 2.1.2) with a 33$^{\text{rd}}$ percentile for selecting the highest concentrations, show that the method is never able to retrieve the emissions sources of the tracers. Conversely, the 5$^{\text{th}}$ percentile does not select enough data points, leading to a miss detection of some of the main source regions. Finally, the 10$^{\text{th}}$ percentile, used by the standard ratio method, gives the best performances when used with one or two years long series of daily measurements.

### 4.2 Series duration

The original experiment had a duration of twenty-four months which corresponds to a complete double seasonal cycle. The sensitivity of the method to the duration and frequency of the concentration series is tested by reducing the number of points of the series. First, in order to test the sensitivity of the method to the time series duration, the experiment is reproduced on two periods of twelve months: on the first year and then on the second one. Then, in order to test the sensitivity of the method to the concentration sampling frequency, the concentration series is cropped to keep only one concentration point every two days. In other words, the number of points is divided by two keeping the same time extent than the original experiment (half frequency). Finally, only one point is kept every week (frequency divided by seven).

The results show that two years analysis does not improve the precision of the method compared to one year experiment. However, a difference is observed when measurements are only performed every two days: the success level loses one point on average. Furthermore, lowering the frequency of measurement down to one every week causes to loose one additional level of success. In conclusion, increasing the time resolution enhances the method's performances. The sampling frequency should always be considered when applying the improved ratio method.

### 4.3 FPES filtering

The improved ratio method (Sect. 3.3) incorporates a filter to exclude the grid cells with the lowest FPES values – i.e., those penetrated by the fewest trajectories. This serves to remove the least statistically significant results, as well as particle dispersion modeling imprecision near the domain boundaries. In practice, FPES values are filtered by a threshold determined after a percentage of the total FPES in the domain for a given case. The threshold should be kept as low as possible in order to avoid information loss. Nevertheless, when it is too low, some arbitrary results may remain. In order to evaluate the effect of this FPES threshold on the performance of the sources detection method, seven thresholds are tested, from no filter to filtering 6 % of the lowest FPES values. Increasing the level of filtering shrinks the studied region around the starting point of the backward dispersion, i.e. the measurement station. Therefore, and because the selected stations are located around the Arctic basin, as the filtering level increases, the representation of the sea ice regions get stronger. In terms of success level of detection, it improves the scores for the sea ice tracer, but tends to lower them for the open ocean (Fig. 7a). Because the tests are performed on simulated tracers (Sect. 2), it is possible to use these findings to calibrate what threshold may give the most reliable and meaningful results for all tracers. In Sect. 3.1, the detection is rated as successful when the $D_T$ score is superior or equal to two. On Fig. 7b, one is counted for every detection that satisfies the above condition (i.e. $D_T \geq 2$). Therefore, a given tracer can have a maximum overall score of five (i.e. a successful detection for the five stations). The evolution of the scores on Fig. 7b shows that a filtering of 2 % is the optimal compromise. It is the lowest threshold for which the total score plateaus. Although the scores for sea ice and continent reverse at a 3 % filter, this does not affect the total score, making it preferable to maintain the lowest possible filtering threshold. Consequently, for the Arctic domain studied in this paper, we recommend to use a 2 % filtering threshold.

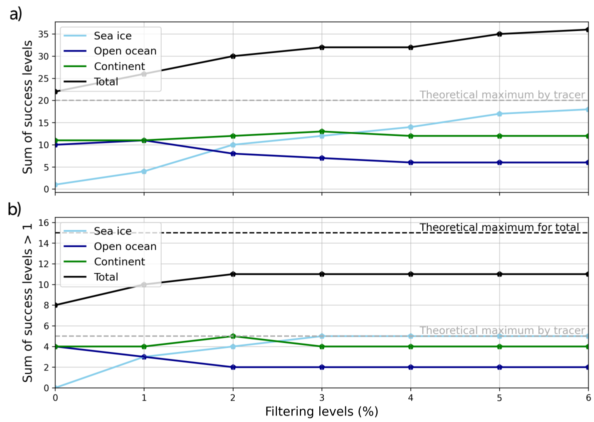


**Figure 7.** Evolution of the success levels sum for different levels of low FPES filtering. On (a), the sum is performed on the scores of the five studied stations (Alert, Ny-Ålesund, Tiksi, Utqiaġvik, Villum) independently for the three tracers (sea ice, open ocean, continent). The total success level is shown in black line. Panel (b) takes only the success levels superior or equal to 2 and sets it to 1. Dashed-lines represent the theoretical maxima of the individual tracers score (gray) and of the total score (black).

## 5 Application examples on aerosol observational datasets

The improved ratio method presented in Sect. 3.3 has shown its capabilities in identifying the type (sea ice, open ocean, continent) of the emission sources of simulated atmospheric tracers. In this section, the method is applied to two observational datasets in order to test it under real conditions. The origin of the species observed in both datasets is well-defined: the first is continental, and the second is oceanic. This knowledge allows for a critical evaluation of the method's results. Discussing the results will provide clarity on how to apply the method correctly and accurately interpret its findings.

### 5.1 Aerosol absorption coefficient

The first dataset is a series of aerosol absorption coefficient measured at the Mount Zeppelin Observatory (Ny-Ålesund, Svalbard) at an altitude of 475 $\mathrm{m}$ above sea level, between January 2019 and September 2022 (Eleftheriadis, 2019). For the application we chose a two years period (September 2019 to August 2021), identical to the period on which the evaluation experiment has been held (Sect. 2.1.2). Aerosol absorption coefficient measured at 550 $\mathrm{nm}$ is known to be mostly driven by black carbon (BC) concentrations as it is by far the strongest absorbing aerosol species in the visible spectrum (Bond et al., 2013; Kirchstetter et al., 2004). Consequently, we consider the aerosol absorption coefficient as a marker of BC. BC is a great candidate for a first application of the method because its sources are relatively well known. Ninety percent of the BC emissions are produced by continental sources, mainly biomass burning and incomplete combustion of fossil fuels from traffic and industrial activities (Bond et al., 2013).

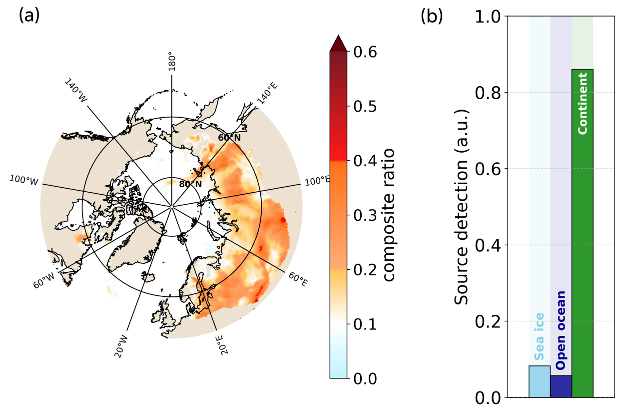


**Figure 8.** Results of the improved ratio method when applied on a data series of absorption coefficient measured at the Zeppelin Observatory (Ny-Ålesund, Svalbard). (a) is the ratio of the improved method that highlights the likely regions of origins. (b) is the quantification of the surface types contributions to the three sources (sea ice, open ocean, continent).

Figure 8 shows the ratio of the improved method as presented in Sect. 3.3 alongside the contribution of sea ice, open ocean and continental regions to the detection signal. Panel (a) highlights a strong Eurasian signal spreading from Northern Europe all the way to eastern Siberia. Panel (b) confirms the continental origin showing that more than 80 % of the signal comes from continental regions. Figure 4b showed that the detection of a continental originated species at Ny-Ålesund could give spurious signal of oceanic regions (sea ice and open ocean). Therefore, the weak oceanic signals showed on panel (b) can be considered as detection noise. The application of the improved ratio method to this series of BC measurements at Zeppelin station unequivocally leads to the conclusion of a continental origin of the observed BC in Svalbard. This finding corroborates the results described in Winiger et al. (2016), Hirdman et al. (2010) and Xu et al. (2017), i.e. BC observed at high-altitude sites comes from remote locations, mainly associated with Eurasian emissions.

### 5.2 Methanesulfonic acid

Methanesulfonic acid (MSA) is an organosulfuric compound. Its presence in the atmosphere is due to the emissions of dimethylsulfide (DMS). DMS is produced by marine bacteria and phytoplankton activity and can be oxidized into MSA in the atmosphere (Saltzman et al., 1983; Hopkins et al., 2023). Therefore, MSA measurements are expected to be associated with air masses of marine origins. Here, the dataset is a series of MSA particle phase measurements performed in the context of the Ny-Ålesund Aerosol Cloud Experiment (NASCENT) campaign held in Svalbard between September 2019 and August

2020 (Pasquier et al., 2022). The measurement series used in this study extends from January to December 2020. However, data is missing between July and August due to an instrument failure (Siegel et al., 2023). Similarly to the BC measurements (Sect. 5.1), the MSA measurements have been done at the Zeppelin Observatory.

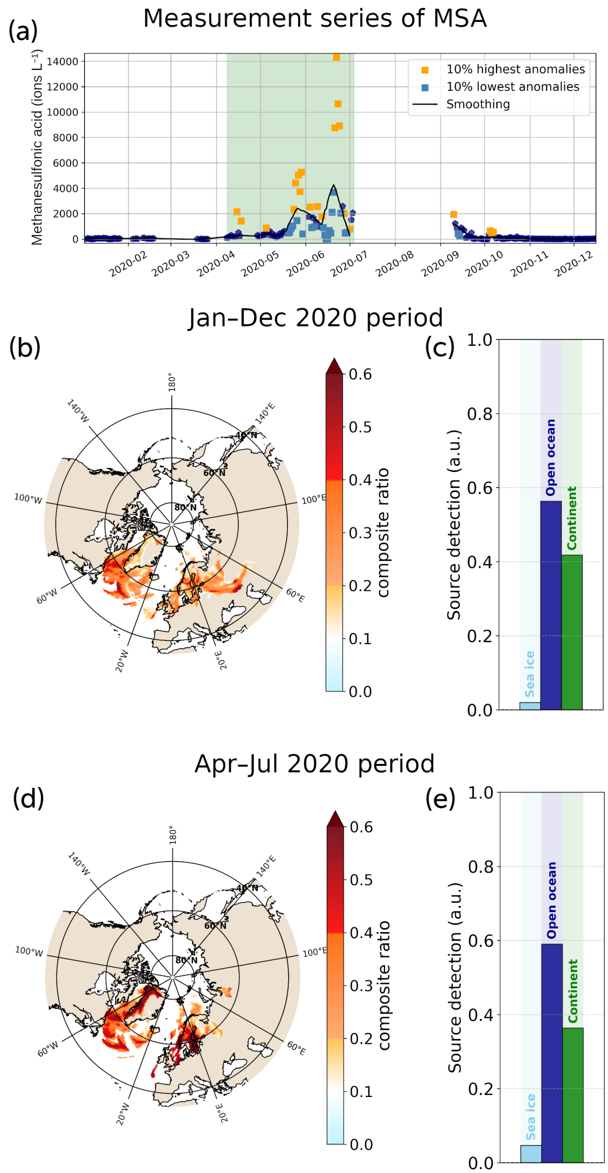


**Figure 9.** Results of the improved ratio method when applied on the data series of Methanesulfonic acid (MSA) measured at Zeppelin Observatory. (a) is the measurement series of MSA over 2020. The points corresponding to the 10 % strongest anomalies are represented in orange (high anomaly) and light blue (low anomaly) squares. (b) and (c) show the results for the complete series of measurements (January to December 2020). (d) and (e) show the results for a period of continuous measurements of the dataset (April to early July).

The analysis of the results shown in Fig. 9 is non-trivial and should be taken as a textbook case of source identification by the ratio method. Panels (b) and (c) show the results for the analysis of the complete dataset extending on the whole 2020 year, while panels (d) and (e) show the results for the measurements between April and early July 2020. Panel (c) shows that, for the whole period of measurements, the main contribution is oceanic, but followed closely by the continental signal, while the sea ice regions contribution amounts to almost zero. The ratio map shown on panel (b) indicates that two main spots stand out. The western one shows strong signal on the Baffin Bay, Labrador Sea and Greenland Sea. Despite some overflow on continental areas, this spot mainly contributes to the oceanic signal, and should be interpreted as such. The second spot spreads over Northern and Eastern Europe. Signal comes from the regions of the North Sea and Baltic Sea which are both regions of high chlorophyll-*a* (Chl-*a*) concentrations. Nevertheless, the main signal of this spot is over continental areas. A part of it may be ascribed to overflows, but the eastern strip has to be considered as an actual signal. It points toward the north of the Caspian Sea, where the phytoplankton might be important (Eker, 2005). Such long range transport is surprising but not impossible: long-range transport of aerosols to the Arctic from Central Eurasia has been observed in the past (Marelle et al., 2015) and the typical lifetime of aerosol MSA against OH oxidation is a few weeks (Mungall et al., 2018). However, no study reports DMS or MSA emissions from this region, and it would be speculative to conclude on a contribution of Caspian Sea origins for the MSA observed at Zeppelin Observatory during this period.

Alternatively, the analysis of the individual FPES plumes teaches that this eastern continental spot is due to three consecutive dates in mid-October (Fig. 9a). Despite the fact that they correspond to low measurement values regarding the observed MSA summer peak, they happen to be flagged as high seasonal anomalies in the measurement series. This is due to the very low levels of MSA observed after mid-September. The absence of measurements over July and August produces a lack of representativeness for the high summer values, which explains why these three dates stand out.

On Fig. 9d and Fig. 9e, the method is applied on the three months period of high MSA activity between April and early July (green period on Fig. 9a). Oceanic regions previously identified remain and are even better highlighted (Fig. 9d). Consequently, the contribution from open ocean regions increases while the continental signal decreases (Fig. 9e). The latter is now mainly due to overflows over Greenland. Although they are spatially limited, such overflows are associated with strong signal values, which is significantly boosting the continental contribution because the statistical representativeness dropped due the series cropping. Let us remind that the detection of oceanic source at Ny-Ålesund can be polluted by 25 % of spurious continental signal (Fig. 4b). Additionally, some Northern Russia signal spots remain. They could be associated with the Barents Sea high phytoplankton coastal activity. But their size and strength do not allow such conclusion since the method does not present high enough spatial precision.

Eventually, the results presented in Fig. 9d and Fig. 9e suggest an oceanic origin of the MSA measured at Zeppelin Observatory between January and July 2020. We identified two main source regions: the western North Atlantic (Greenland Sea, Labrador Sea and Baffin Bay), and the North Sea/Baltic Sea, which is in great accordance with the results of Pernov et al. (2024) for the corresponding season. Furthermore, these conclusions are consistent with the Chl-*a* observations during the studied period (NASA Ocean Biology Processing Group, 2022).

## 6 Conclusions

This study aimed to introduce an enhanced and evaluated methodology for tracing the sources of atmospheric species using backward modeling, with a focus on the Arctic region. We adapted the method presented by Hirdman et al. (2010), and took advantage of the FLEXPART PES plume representation inherent to LPDMs, in order to provide deepened information on the potential sources than classical single backtrajectory analysis would do. Named after its principal characteristic, the ratio method (or PSCF) relies on the identification of the deviation of the air masses origins associated with the highest observed concentrations, from the climatology of air mass origins for a given measurement station and time period.

To get insight of the performances of the ratio method, we analyzed simulated data of idealized tracers emitted within WRF-Chem from three different surface types : the Arctic sea ice, and the open ocean and continental regions. The complete knowledge of the simulated tracers emissions allowed to continuously assess the performances of the source detection method, along with its sensibility to a set of parameters. This context made it possible to refine the methodology.

Testing the approach of the standard ratio method on simulated data showed it is unreliable for the identification of the simulated tracers origins, and therefore for identifying source regions of short-lived atmospheric species. The reasons for this lack of reliability and the responses we have tested are listed hereinbelow, by order of decreasing importance.

- The results are highly dependent on the percentile threshold used to sort the concentrations between the highest and lowest measurements. While the 33$^{\text{th}}$ percentile has been used in the literature without being strictly evaluated (Irish et al., 2019), our results shows that such a high threshold can not be used to identify likely sources with confidence. We recommend to select the 10 % highest values, which implies to have sufficiently long time series. Although some conclusions of previous works may be right, they should be re-evaluated with the improved ratio method presented here.

- The results of the standard ratio method are influenced by the geographical and layout wind configuration, causing an over-representation of the continental areas and a shadowing effect in the detected sources. We introduced a filter on the lowest FPES values in order to eliminate the less statistically significant ones. It led to a better representation of the three surface types, which resulted in a dramatic improvement of the detection results. The effect of this filtering is to shrink the result of the method close to the measurement station. The variability of improvement between the different stations and tracers suggests that the parameters we used might not be generalized for other regions or compounds, although the methodology to get the best filtering level can be generalized.

- The standard ratio method can either seek the sources or the sinks regions of a studied species, but the results stay independent. With the improved ratio method, we created a novel approach by introducing a composite ratio that takes advantage of the information contained in the detection signal associated with both the highest and the lowest measurements. With the improved ratio method, we introduced a composite ratio that takes advantage of the information contained in the detection signal associated to both the highest and the lowest measurements.

– We found that sorting the raw concentrations between highest and lowest values was seasonally biased by the underlying annual cycle. We updated the method to instead sort concentration anomalies after subtracting the low-frequency annual cycle.

The idealized tracer experiment setup for the evaluation of the identification method with LDPM presents several limitations. One of them, inherent to our evaluation protocol, is the choice of the dispersion modeling duration. We set up FLEXPART-WRF to follow the air masses pathways seven days back in time, which was coherent with the lifetime of our simulated tracers. Therefore, the improved method we developed is optimized for short-lived atmospheric species. Using the method thus implies to make assumption on the lifetime of the studied species. An extended evaluation would explore how the ratio method performs with long-lived species, which was not in the frame of this study. A related point is the setup of removal processes for the evaluation experiment. A removal by exponential decay was used to represent short-lived species. This causes two important limitations: 1) the uncertainties on removal processes are not taken into account in the results, 2) the present evaluation does not explore the effects of different removal processes on the performance of the method. Consequently, one should pay special attention to what removal parameterization is set in the LPDM when attempting an emission source identification. Our evaluation has been specific to the Arctic region. Consequently, some parameters of the improved ratio method – especially the FPES filter – are set for best performance in the northern high latitudes. For other regions, with different geographical layouts, the FPES filtering may need to be adjusted with an other simulated experiment, similar to the one presented in this study. We recall that the FPES filter is mainly used to restore balance to the representations of the different surface types (sea ice, open ocean, continent) in the domain. In lower latitude domains, the FPES filter could be of less importance. Regarding the limitations of the backward modelling approaches, the intrinsic uncertainties of the backtrajectory models and LPDMs can not be cleared of. Since backward modelling rely on simulated meteorological fields, the precision of the source detection suffers from both the errors of the Lagrangian model and those of the weather model or reanalysis. However, we eliminated the latter in our evaluation experiment since we use the same model to produce the data and to feed the LPDM.

The tests performed on this advanced ratio method showed it can give useful information on the origins of atmospheric species, even though this kind of approach has inherent limitations. The results presented here allow to estimate the magnitude of these limitations in order to adopt a critical look on any result from real applications of the method.

The assessment of the method time resolution (frequency of measurement points) sensitivity showed that series of daily measurements give better results than series of lower frequency, and therefore should be privileged for applying the method. Combining simultaneous observations of the same species at different locations can also help to give more precise source detection, and should be encouraged for future campaigns.

The evaluation led in this study allowed with a unique modeling approach to quantify the source detection performances of the ratio method inspired by Hirdman et al. (2010), and as it has been used in several research articles (eg. Irish et al., 2019; Si et al., 2019). Although this standard ratio method is more advanced than most of the backward trajectory analysis used in studies about short-lived atmospheric species (Allen et al., 2021; An et al., 2014; Hartmann et al., 2021; Lu et al., 2012;

Porter et al., 2022; Raut et al., 2017; Wex et al., 2019), the assessment results have shown that its performances are insufficient for identifying unknown emission sources. Conversely, our improved ratio method is able to retrieve the source regions of an observed atmospheric species with an unprecedented precision. The demonstrated performances instill confidence to use the method in order to identify unknown sources and to confirm presumed ones.

Because backward modeling analysis for source identification is widely used, the results presented here impact many past and future studies. The new analysis protocol for emission origins detection presented alongside the performance evaluation may find its application in a wide range of atmospheric studies. Here we show an Arctic application, but the conclusions should be general for short-lived atmospheric species in other regions. Therefore testing and adoption of this method in other regions is encouraged.

## Appendix A

### WRF setup

| **Physics and Meteorology** | **Model Option** |
|---|---|
| Planetary boundary layer / Surface layer | MYNN level 2.5 TKE scheme / MYNN (Nakanishi and Niino, 2009) |
| Surface layer | Noah LSM (Tewari et al., 2004) |
| Microphysics | Morrison (Morrison et al., 2009) |
| SW/LW radiation | RRTMG (Iacono et al., 2008) |
| Cumulus | Grell-3 (Grell and Dévényi, 2002) |
| Initial and boundary conditions | NCEP FNL (Commerce, 2000) |

**Table A1.** WRF model setup

**Table A2.** Comparison of the success levels of the standard ratio method (standard) and the improved method (improved) for the evaluation experiment performed on five stations and three tracers. Bold numbers indicate which method scored better.

| Stations | Sea ice tracer | | Open ocean tracer | | Continental tracer | |
|---|---|---|---|---|---|---|
| | standard | improved | standard | improved | standard | improved |
| Alert | 0 | **1** | 0 | **2** | 2 | 2 |
| Ny-Ålesund | 0 | **1** | 2 | **3** | 2 | 2 |
| Tiksi | 0 | **3** | **1** | 0 | 2 | **4** |
| Utqiaġvik | 0 | **2** | 0 | **1** | 2 | 2 |
| Villum | 0 | **2** | 2 | **3** | 0 | **2** |

*Code and data availability.* The python scripts for running the Improved Ratio Method as described in this article, as well as an example test case on a simulated tracer, are available in the following Zenodo repository: https://doi.org/10.5281/zenodo.13902693. The aerosol absorption coefficient dataset (Eleftheriadis, 2019) is hosted on the EBAS open access database.

*Author contributions.* ADS performed the simulations, developed the analysis tools and drafted the manuscript. LM, JCR and JT provided scientific support and research ideas while supervising the study. YG, KS, SH and CM provided the dataset of methanesulfonic acid and performed the field measurements. All the authors contributed to the final version of the text.

*Competing interests.* The authors declare that they have no conflict of interest.

*Acknowledgements.* Computer modelling benefited from access to IDRIS HPC resources (GENCI allocations A013017141 and A0150170141) and the IPSL mesoscale computing center. We acknowledge use of the WRF-Chem preprocessor tool (mozbc, fire_emiss, bio_emiss, anthro_emiss) provided by the Atmospheric Chemistry Observations and Modeling Lab (ACOM) of NCAR. We thank the Norwegian Institute for Air Research (NILU) for operating the EBAS database, and we thank Eleftheriadis (2019) for providing their data in open access. We would also like to thank the numerous developers who contributed to the free and open-source tools used for the data visualization and analysis, in particular Matplotlib (Hunter, 2007), Cartopy (Met Office, 2010) and xarray (Hoyer and Hamman, 2017). Finally, the authors sincerely thank the two anonymous referees for their helpful comments and suggestions, which helped improve the paper.

*Financial support.* This project has received funding from the European Union's Horizon 2020 research and innovation program under grant agreement no. 101003816 via project CRiceS (Climate Relevant interactions and feedbacks : the key role of sea ice and Snow in the polar and global climate system), and from the Horizon Europe program under grant agreement no. 101137680 via project CERTAINTY (Cloud-aERosol inTeractions their impActs IN The earth sYstem). This work is a contribution to the (MPC)2 project, supported by the Agence Nationale de la Recherche under the Grant ANR-22-CE01-0009.

## References


Allen, S., Allen, D., Baladima, F., Phoenix, V. R., Thomas, J. L., Le Roux, G., and Sonke, J. E.: Evidence of free tropospheric and long-range transport of microplastic at Pic du Midi Observatory, Nature Communications, 12, 7242, https://doi.org/10.1038/s41467-021-27454-7, publisher: Nature Publishing Group, 2021.

An, X., Yao, B., Li, Y., Li, N., and Zhou, L.: Tracking source area of Shangdianzi station using Lagrangian particle dispersion model of FLEXPART, Meteorological Applications, 21, 466–473, https://doi.org/10.1002/met.1358, _eprint: https://onlinelibrary.wiley.com/doi/pdf/10.1002/met.1358, 2014.

Ashbaugh, L. L.: A Statistical Trajectory Technique for Determining Air Pollution Source Regions, Journal of the Air Pollution Control Association, 33, 1096–1098, https://doi.org/10.1080/00022470.1983.10465702, publisher: Taylor & Francis _eprint: https://doi.org/10.1080/00022470.1983.10465702, 1983.

Ashbaugh, L. L., Malm, W. C., and Sadeh, W. Z.: A residence time probability analysis of sulfur concentrations at grand Canyon National Park, Atmospheric Environment (1967), 19, 1263–1270, https://doi.org/10.1016/0004-6981(85)90256-2, 1985.

Bond, T. C., Doherty, S. J., Fahey, D. W., Forster, P. M., Berntsen, T., DeAngelo, B. J., Flanner, M. G., Ghan, S., Kärcher, B., Koch, D., Kinne, S., Kondo, Y., Quinn, P. K., Sarofim, M. C., Schultz, M. G., Schulz, M., Venkataraman, C., Zhang, H., Zhang, S., Bellouin, N., Guttikunda, S. K., Hopke, P. K., Jacobson, M. Z., Kaiser, J. W., Klimont, Z., Lohmann, U., Schwarz, J. P., Shindell, D., Storelvmo, T., Warren, S. G., and Zender, C. S.: Bounding the role of black carbon in the climate system: A scientific assessment, Journal of Geophysical Research: Atmospheres, 118, 5380–5552, https://doi.org/10.1002/jgrd.50171, _eprint: https://onlinelibrary.wiley.com/doi/pdf/10.1002/jgrd.50171, 2013.

Brioude, J., Arnold, D., Stohl, A., Cassiani, M., Morton, D., Seibert, P., Angevine, W., Evan, S., Dingwell, A., Fast, J. D., Easter, R. C., Pisso, I., Burkhart, J., and Wotawa, G.: The Lagrangian particle dispersion model FLEXPART-WRF version 3.1, Geoscientific Model Development, 6, 1889–1904, https://doi.org/10.5194/gmd-6-1889-2013, 2013.

Bronselaer, B., Winton, M., Griffies, S. M., Hurlin, W. J., Rodgers, K. B., Sergienko, O. V., Stouffer, R. J., and Russell, J. L.: Change in future climate due to Antarctic meltwater, Nature, 564, 53–58, https://doi.org/10.1038/s41586-018-0712-z, number: 7734 Publisher: Nature Publishing Group, 2018.

Brunner, D., Henne, S., Keller, C. A., Vollmer, M. K., Reimann, S., and Buchmann, B.: Estimating European Halocarbon Emissions Using Lagrangian Backward Transport Modeling and in Situ Measurements at the Jungfraujoch High-Alpine Site, in: Lagrangian Modeling of the Atmosphere, pp. 207–222, American Geophysical Union (AGU), ISBN 978-1-118-70457-8, https://doi.org/10.1029/2012GM001258, section: 18 _eprint: https://onlinelibrary.wiley.com/doi/pdf/10.1029/2012GM001258, 2012.

Burrows, S. M., Hoose, C., Pöschl, U., and Lawrence, M. G.: Ice nuclei in marine air: biogenic particles or dust?, Atmospheric Chemistry and Physics, 13, 245–267, https://doi.org/10.5194/acp-13-245-2013, 2013.

Carslaw, K. S., La, L., Cl, R., Kj, P., A, R., Pm, F., Gw, M., Dv, S., Mt, W., La, R., and Jr, P.: Large contribution of natural aerosols to uncertainty in indirect forcing, Nature, 503, https://doi.org/10.1038/nature12674, publisher: Nature, 2013.

Cassiani, M., Stohl, A., Olivié, D., Seland, , Bethke, I., Pisso, I., and Iversen, T.: The offline Lagrangian particle model FLEXPART–NorESM/CAM (v1): model description and comparisons with the online NorESM transport scheme and with the reference FLEXPART model, Geoscientific Model Development, 9, 4029–4048, https://doi.org/10.5194/gmd-9-4029-2016, publisher: Copernicus GmbH, 2016.

Commerce, N. C. f. E. P. W. S. S. D. o.: NCEP FNL Operational Model Global Tropospheric Analyses, continuing from July 1999, https://doi.org/10.5065/D6M043C6, 2000.

Dubovik, O., Lapyonok, T., Kaufman, Y. J., Chin, M., Ginoux, P., Kahn, R. A., and Sinyuk, A.: Retrieving global aerosol sources from satellites using inverse modeling, Atmospheric Chemistry and Physics, 8, 209–250, https://doi.org/10.5194/acp-8-209-2008, publisher: Copernicus GmbH, 2008.

Eker, E.: Phytoplankton distribution in the Caspian Sea during March 2001, Hydrobiologia, https://www.academia.edu/4864147/Phytoplankton_distribution_in_the_Caspian_Sea_during_March_2001, 2005.

Eleftheriadis, K.: Aerosol absorption coefficient - filter absorption photometer at Zeppelin mountain (Ny-Ålesund), 2019.

Fang, X., Stohl, A., Yokouchi, Y., Kim, J., Li, S., Saito, T., Park, S., and Hu, J.: Multiannual Top-Down Estimate of HFC-23 Emissions in East Asia, Environmental Science & Technology, 49, 4345–4353, https://doi.org/10.1021/es505669j, publisher: American Chemical Society, 2015.

Fang, X., Saito, T., Park, S., Li, S., Yokouchi, Y., and Prinn, R. G.: Performance of Back-Trajectory Statistical Methods and Inverse Modeling Method in Locating Emission Sources, ACS Earth and Space Chemistry, 2, 843–851, https://doi.org/10.1021/acsearthspacechem.8b00062, publisher: American Chemical Society, 2018.

Farmer, D. K., Boedicker, E. K., and DeBolt, H. M.: Dry Deposition of Atmospheric Aerosols: Approaches, Observations, and Mechanisms, Annual Review of Physical Chemistry, 72, 375–397, https://doi.org/10.1146/annurev-physchem-090519-034936, 2021.

Freitas, G. P., Stolle, C., Kaye, P. H., Stanley, W., Herlemann, D. P. R., Salter, M. E., and Zieger, P.: Emission of primary bioaerosol particles from Baltic seawater, Environmental Science: Atmospheres, 2, 1170–1182, https://doi.org/10.1039/D2EA00047D, publisher: RSC, 2022.

Ginoux, P., Chin, M., Tegen, I., Prospero, J. M., Holben, B., Dubovik, O., and Lin, S.-J.: Sources and distributions of dust aerosols simulated with the GOCART model, Journal of Geophysical Research: Atmospheres, 106, 20 255–20 273, https://doi.org/10.1029/2000JD000053, _eprint: https://onlinelibrary.wiley.com/doi/pdf/10.1029/2000JD000053, 2001.

Gong, X., Zhang, J., Croft, B., Yang, X., Frey, M. M., Bergner, N., Chang, R. Y.-W., Creamean, J. M., Kuang, C., Martin, R. V., Ranjithkumar, A., Sedlacek, A. J., Uin, J., Willmes, S., Zawadowicz, M. A., Pierce, J. R., Shupe, M. D., Schmale, J., and Wang, J.: Arctic warming by abundant fine sea salt aerosols from blowing snow, Nature Geoscience, 16, 768–774, https://doi.org/10.1038/s41561-023-01254-8, number: 9 Publisher: Nature Publishing Group, 2023.

Grell, G. A. and Dévényi, D.: A generalized approach to parameterizing convection combining ensemble and data assimilation techniques, Geophysical Research Letters, 29, 38–1–38–4, https://doi.org/10.1029/2002GL015311, 2002.

Grell, G. A., Peckham, S. E., Schmitz, R., McKeen, S. A., Frost, G., Skamarock, W. C., and Eder, B.: Fully coupled “online” chemistry within the WRF model, Atmospheric Environment, 39, 6957–6975, https://doi.org/https://doi.org/10.1016/j.atmosenv.2005.04.027, 2005.

Hartmann, M., Adachi, K., Eppers, O., Haas, C., Herber, A., Holzinger, R., Hünerbein, A., Jäkel, E., Jentzsch, C., van Pinxteren, M., Wex, H., Willmes, S., and Stratmann, F.: Wintertime Airborne Measurements of Ice Nucleating Particles in the High Arctic: A Hint to a Marine, Biogenic Source for Ice Nucleating Particles, Geophysical Research Letters, 47, e2020GL087 770, https://doi.org/10.1029/2020GL087770, _eprint: https://onlinelibrary.wiley.com/doi/pdf/10.1029/2020GL087770, 2020.

Hartmann, M., Gong, X., Kecorius, S., van Pinxteren, M., Vogl, T., Welti, A., Wex, H., Zeppenfeld, S., Herrmann, H., Wiedensohler, A., and Stratmann, F.: Terrestrial or marine – indications towards the origin of ice-nucleating particles during melt season in the European Arctic up to 83.7° N, Atmospheric Chemistry and Physics, 21, 11 613–11 636, https://doi.org/10.5194/acp-21-11613-2021, publisher: Copernicus GmbH, 2021.

Hegarty, J., Draxler, R. R., Stein, A. F., Brioude, J., Mountain, M., Eluszkiewicz, J., Nehrkorn, T., Ngan, F., and Andrews, A.: Evaluation of Lagrangian Particle Dispersion Models with Measurements from Controlled Tracer Releases, Journal of Applied Meteorology and Climatology, 52, 2623–2637, https://doi.org/10.1175/JAMC-D-13-0125.1, publisher: American Meteorological Society Section: Journal of Applied Meteorology and Climatology, 2013.

Heutte, B., Bergner, N., Angot, H., Pernov, J. B., Dada, L., Mirrielees, J. A., Beck, I., Baccarini, A., Boyer, M., Creamean, J. M., Daellenbach, K. R., El Haddad, I., Frey, M. M., Henning, S., Laurila, T., Moschos, V., Petäjä, T., Pratt, K. A., Quéléver, L. L. J., Shupe, M. D., Zieger, P., Jokinen, T., and Schmale, J.: Observations of high-time-resolution and size-resolved aerosol chemical composition and microphysics in the central Arctic: implications for climate-relevant particle properties, Atmospheric Chemistry and Physics, 25, 2207–2241, https://doi.org/10.5194/acp-25-2207-2025, publisher: Copernicus GmbH, 2025.

Hirdman, D., Aspmo, K., Burkhart, J. F., Eckhardt, S., Sodemann, H., and Stohl, A.: Transport of mercury in the Arctic atmosphere: Evidence for a spring-time net sink and summer-time source, Geophysical Research Letters, 36, https://doi.org/https://doi.org/10.1029/2009GL038345, _eprint: https://agupubs.onlinelibrary.wiley.com/doi/pdf/10.1029/2009GL038345, 2009.

Hirdman, D., Sodemann, H., Eckhardt, S., Burkhart, J. F., Jefferson, A., Mefford, T., Quinn, P. K., Sharma, S., Ström, J., and Stohl, A.: Source identification of short-lived air pollutants in the Arctic using statistical analysis of measurement data and particle dispersion model output, Atmospheric Chemistry and Physics, 10, 669–693, https://doi.org/10.5194/acp-10-669-2010, 2010.

Hopkins, F. E., Archer, S. D., Bell, T. G., Suntharalingam, P., and Todd, J. D.: The biogeochemistry of marine dimethylsulfide, Nature Reviews Earth & Environment, 4, 361–376, https://doi.org/10.1038/s43017-023-00428-7, publisher: Nature Publishing Group, 2023.

Hoyer, S. and Hamman, J.: xarray: N-D labeled Arrays and Datasets in Python, Journal of Open Research Software, 5, https://doi.org/10.5334/jors.148, 2017.

Hsu, Y.-K., Holsen, T. M., and Hopke, P. K.: Comparison of hybrid receptor models to locate PCB sources in Chicago, Atmospheric Environment, 37, 545–562, https://doi.org/10.1016/S1352-2310(02)00886-5, 2003.

Hunter, J. D.: Matplotlib: A 2D Graphics Environment, Computing in Science & Engineering, 9, 90–95, https://doi.org/10.1109/MCSE.2007.55, conference Name: Computing in Science & Engineering, 2007.

Iacono, M. J., Delamere, J. S., Mlawer, E. J., Shephard, M. W., Clough, S. A., and Collins, W. D.: Radiative forcing by long-lived greenhouse gases: Calculations with the AER radiative transfer models, Journal of Geophysical Research: Atmospheres, 113, https://doi.org/10.1029/2008JD009944, _eprint: https://onlinelibrary.wiley.com/doi/pdf/10.1029/2008JD009944, 2008.

IPCC: The Sixth Assessment Report, Climate Change 2021: The Physical Science Basis, Tech. rep., https://www.ipcc.ch/report/sixth-assessment-report-working-group-i/, 2021.

Irish, V. E., Hanna, S. J., Willis, M. D., China, S., Thomas, J. L., Wentzell, J. J. B., Cirisan, A., Si, M., Leaitch, W. R., Murphy, J. G., Abbatt, J. P. D., Laskin, A., Girard, E., and Bertram, A. K.: Ice nucleating particles in the marine boundary layer in the Canadian Arctic during summer 2014, Atmospheric Chemistry and Physics, 19, 1027–1039, https://doi.org/10.5194/acp-19-1027-2019, 2019.

Jiang, J. H., Su, H., Massie, S. T., Colarco, P. R., Schoeberl, M. R., and Platnick, S.: Aerosol-CO relationship and aerosol effect on ice cloud particle size: Analyses from Aura Microwave Limb Sounder and Aqua Moderate Resolution Imaging Spectroradiometer observations, Journal of Geophysical Research: Atmospheres, 114, https://doi.org/10.1029/2009JD012421, _eprint: https://onlinelibrary.wiley.com/doi/pdf/10.1029/2009JD012421, 2009.

Jones, A., Thomson, D., Hort, M., and Devenish, B.: The U.K. Met Office's Next-Generation Atmospheric Dispersion Model, NAME III, in: Air Pollution Modeling and Its Application XVII, edited by Borrego, C. and Norman, A.-L., pp. 580–589, Springer US, Boston, MA, ISBN 978-0-387-68854-1, https://doi.org/10.1007/978-0-387-68854-1_62, 2007.

Kirchstetter, T. W., Novakov, T., and Hobbs, P. V.: Evidence that the spectral dependence of light absorption by aerosols is affected by organic carbon, Journal of Geophysical Research: Atmospheres, 109, https://doi.org/10.1029/2004JD004999, _eprint: https://onlinelibrary.wiley.com/doi/pdf/10.1029/2004JD004999, 2004.

Lapere, R., Marelle, L., Rampal, P., Brodeau, L., Melsheimer, C., Spreen, G., and Thomas, J. L.: Modeling the contribution of leads to sea spray aerosol in the high Arctic, EGUsphere, pp. 1–31, https://doi.org/10.5194/egusphere-2024-1271, publisher: Copernicus GmbH, 2024.

Lu, Z., Streets, D. G., Zhang, Q., and Wang, S.: A novel back-trajectory analysis of the origin of black carbon transported to the Himalayas and Tibetan Plateau during 1996–2010, Geophysical Research Letters, 39, https://doi.org/10.1029/2011GL049903, _eprint: https://onlinelibrary.wiley.com/doi/pdf/10.1029/2011GL049903, 2012.

Manning, A. J., O'Doherty, S., Jones, A. R., Simmonds, P. G., and Derwent, R. G.: Estimating UK methane and nitrous oxide emissions from 1990 to 2007 using an inversion modeling approach, Journal of Geophysical Research: Atmospheres, 116, https://doi.org/10.1029/2010JD014763, _eprint: https://onlinelibrary.wiley.com/doi/pdf/10.1029/2010JD014763, 2011.

Marelle, L., Raut, J.-C., Thomas, J. L., Law, K. S., Quennehen, B., Ancellet, G., Pelon, J., Schwarzenboeck, A., and Fast, J. D.: Transport of anthropogenic and biomass burning aerosols from Europe to the Arctic during spring 2008, Atmospheric Chemistry and Physics, 15, 3831–3850, https://doi.org/10.5194/acp-15-3831-2015, publisher: Copernicus GmbH, 2015.

Marelle, L., Raut, J.-C., Law, K. S., Berg, L. K., Fast, J. D., Easter, R. C., Shrivastava, M., and Thomas, J. L.: Improvements to the WRF-Chem 3.5.1 model for quasi-hemispheric simulations of aerosols and ozone in the Arctic, Geoscientific Model Development, 10, 3661–3677, https://doi.org/10.5194/gmd-10-3661-2017, publisher: Copernicus GmbH, 2017.

Matus, A. V. and L'Ecuyer, T. S.: The role of cloud phase in Earth's radiation budget, Journal of Geophysical Research: Atmospheres, 122, 2559–2578, https://doi.org/https://doi.org/10.1002/2016JD025951, 2017.

Met Office: Cartopy: a cartographic python library with a Matplotlib interface, Exeter, Devon, https://scitools.org.uk/cartopy, 2010.

Monahan, E. C., Spiel, D. E., and Davidson, K. L.: A Model of Marine Aerosol Generation Via Whitecaps and Wave Disruption, in: Oceanic Whitecaps: And Their Role in Air-Sea Exchange Processes, edited by Monahan, E. C. and Niocaill, G. M., Oceanographic Sciences Library, pp. 167–174, Springer Netherlands, Dordrecht, ISBN 978-94-009-4668-2, https://doi.org/10.1007/978-94-009-4668-2_16, 1986.

Morrison, H., Thompson, G., and Tatarskii, V.: Impact of Cloud Microphysics on the Development of Trailing Stratiform Precipitation in a Simulated Squall Line: Comparison of One- and Two-Moment Schemes, Monthly Weather Review, 137, 991–1007, https://doi.org/10.1175/2008MWR2556.1, publisher: American Meteorological Society Section: Monthly Weather Review, 2009.

Morrison, H., van Lier-Walqui, M., Fridlind, A. M., Grabowski, W. W., Harrington, J. Y., Hoose, C., Korolev, A., Kumjian, M. R., Milbrandt, J. A., Pawlowska, H., Posselt, D. J., Prat, O. P., Reimel, K. J., Shima, S.-I., van Diedenhoven, B., and Xue, L.: Confronting the Challenge of Modeling Cloud and Precipitation Microphysics, Journal of Advances in Modeling Earth Systems, 12, e2019MS001 689, https://doi.org/10.1029/2019MS001689, _eprint: https://onlinelibrary.wiley.com/doi/pdf/10.1029/2019MS001689, 2020.

Mungall, E. L., Wong, J. P. S., and Abbatt, J. P. D.: Heterogeneous Oxidation of Particulate Methanesulfonic Acid by the Hydroxyl Radical: Kinetics and Atmospheric Implications, ACS Earth and Space Chemistry, 2, 48–55, https://doi.org/10.1021/acsearthspacechem.7b00114, publisher: American Chemical Society, 2018.

Murray, B. J., Carslaw, K. S., and Field, P. R.: Opinion: Cloud-phase climate feedback and the importance of ice-nucleating particles, Atmospheric Chemistry and Physics, 21, 665–679, https://doi.org/10.5194/acp-21-665-2021, 2021.

Möhler, O., Adams, M., Lacher, L., Vogel, F., Nadolny, J., Ullrich, R., Boffo, C., Pfeuffer, T., Hobl, A., Weiß, M., Vepuri, H. S. K., Hiranuma, N., and Murray, B. J.: The Portable Ice Nucleation Experiment (PINE): a new online instrument for laboratory studies and automated long-term field observations of ice-nucleating particles, Atmospheric Measurement Techniques, 14, 1143–1166, https://doi.org/10.5194/amt-14-1143-2021, publisher: Copernicus GmbH, 2021.

Nakanishi, M. and Niino, H.: Development of an Improved Turbulence Closure Model for the Atmospheric Boundary Layer, Journal of the Meteorological Society of Japan. Ser. II, 87, 895–912, https://doi.org/10.2151/jmsj.87.895, 2009.

NASA Ocean Biology Processing Group: Aqua MODIS Level 3 Mapped Chlorophyll Data, Version R2022.0, https://doi.org/10.5067/AQUA/MODIS/L3M/CHL/2022, 2022.

Ohata, S., Moteki, N., Mori, T., Koike, M., and Kondo, Y.: A key process controlling the wet removal of aerosols: new observational evidence, Scientific Reports, 6, 34 113, https://doi.org/10.1038/srep34113, 2016.

Park, K.-T., Jang, S., Lee, K., Yoon, Y. J., Kim, M.-S., Park, K., Cho, H.-J., Kang, J.-H., Udisti, R., Lee, B.-Y., and Shin, K.-H.: Observational evidence for the formation of DMS-derived aerosols during Arctic phytoplankton blooms, Atmospheric Chemistry and Physics, 17, 9665–9675, https://doi.org/10.5194/acp-17-9665-2017, 2017.

Parshintsev, J. and Hyötyläinen, T.: Methods for characterization of organic compounds in atmospheric aerosol particles, Analytical and Bioanalytical Chemistry, 407, 5877–5897, https://doi.org/10.1007/s00216-014-8394-3, 2015.

Partridge, D. G., Vrugt, J. A., Tunved, P., Ekman, A. M. L., Gorea, D., and Sorooshian, A.: Inverse modeling of cloud-aerosol interactions – Part 1: Detailed response surface analysis, Atmospheric Chemistry and Physics, 11, 7269–7287, https://doi.org/10.5194/acp-11-7269-2011, publisher: Copernicus GmbH, 2011.

Pasquier, J. T., David, R. O., Freitas, G., Gierens, R., Gramlich, Y., Haslett, S., Li, G., Schäfer, B., Siegel, K., Wieder, J., Adachi, K., Belosi, F., Carlsen, T., Decesari, S., Ebell, K., Gilardoni, S., Gysel-Beer, M., Henneberger, J., Inoue, J., Kanji, Z. A., Koike, M., Kondo, Y., Krejci, R., Lohmann, U., Maturilli, M., Mazzolla, M., Modini, R., Mohr, C., Motos, G., Nenes, A., Nicosia, A., Ohata, S., Paglione, M., Park, S., Pileci, R. E., Ramelli, F., Rinaldi, M., Ritter, C., Sato, K., Storelvmo, T., Tobo, Y., Traversi, R., Viola, A., and Zieger, P.: The Ny-Ålesund Aerosol Cloud Experiment (NASCENT): Overview and First Results, Bulletin of the American Meteorological Society, 103, E2533–E2558, https://doi.org/10.1175/BAMS-D-21-0034.1, publisher: American Meteorological Society Section: Bulletin of the American Meteorological Society, 2022.

Pernov, J. B., Harris, E., Volpi, M., Baumgartner, T., Hohermuth, B., Henne, S., Aeberhard, W. H., Becagli, S., Quinn, P. K., Traversi, R., Upchurch, L. M., and Schmale, J.: Pan-Arctic Methanesulfonic Acid Aerosol: Source regions, atmospheric drivers, and future projections, https://doi.org/10.21203/rs.3.rs-3976619/v1, iSSN: 2693-5015, 2024.

Pisso, I., Sollum, E., Grythe, H., Kristiansen, N. I., Cassiani, M., Eckhardt, S., Arnold, D., Morton, D., Thompson, R. L., Groot Zwaaftink, C. D., Evangeliou, N., Sodemann, H., Haimberger, L., Henne, S., Brunner, D., Burkhart, J. F., Fouilloux, A., Brioude, J., Philipp, A., Seibert, P., and Stohl, A.: The Lagrangian particle dispersion model FLEXPART version 10.4, Geoscientific Model Development, 12, 4955–4997, https://doi.org/10.5194/gmd-12-4955-2019, 2019.

Polissar, A. V., Hopke, P. K., Paatero, P., Kaufmann, Y. J., Hall, D. K., Bodhaine, B. A., Dutton, E. G., and Harris, J. M.: The aerosol at Barrow, Alaska: long-term trends and source locations, Atmospheric Environment, 33, 2441–2458, https://doi.org/10.1016/S1352-2310(98)00423-3, 1999.

Porter, G. C. E., Adams, M. P., Brooks, I. M., Ickes, L., Karlsson, L., Leck, C., Salter, M. E., Schmale, J., Siegel, K., Sikora, S. N. F., Tarn, M. D., Vüllers, J., Wernli, H., Zieger, P., Zinke, J., and Murray, B. J.: Highly Active Ice-Nucleating Particles at the Summer North Pole, Journal of Geophysical Research: Atmospheres, 127, e2021JD036 059, https://doi.org/https://doi.org/10.1029/2021JD036059, _eprint: https://agupubs.onlinelibrary.wiley.com/doi/pdf/10.1029/2021JD036059, 2022.

Rantanen, M., K. A. L. A.: he Arctic has warmed nearly four times faster than the globe since 1979, Communication Earth Environment, 3, https://doi.org/10.1038/s43247-022-00498-3, 2022.

Raut, J.-C., Marelle, L., Fast, J. D., Thomas, J. L., Weinzierl, B., Law, K. S., Berg, L. K., Roiger, A., Easter, R. C., Heimerl, K., Onishi, T., Delanoë, J., and Schlager, H.: Cross-polar transport and scavenging of Siberian aerosols containing black carbon during the 2012 ACCESS summer campaign, Atmospheric Chemistry and Physics, 17, 10 969–10 995, https://doi.org/10.5194/acp-17-10969-2017, publisher: Copernicus GmbH, 2017.

Ren, B., Xie, P., Xu, J., Li, A., Tian, X., Hu, Z., Huang, Y., Li, X., Zhang, Q., Ren, H., and Ji, H.: Use of the PSCF method to analyze the variations of potential sources and transports of NO2, SO2, and HCHO observed by MAX-DOAS in Nanjing, China during 2019, Science of The Total Environment, 782, 146 865, https://doi.org/10.1016/j.scitotenv.2021.146865, 2021.

Resovsky, A., Ramonet, M., Rivier, L., Tarniewicz, J., Ciais, P., Steinbacher, M., Mammarella, I., Mölder, M., Heliasz, M., Kubistin, D., Lindauer, M., Müller-Williams, J., Conil, S., and Engelen, R.: An algorithm to detect non-background signals in greenhouse gas time series from European tall tower and mountain stations, Atmospheric Measurement Techniques, 14, 6119–6135, https://doi.org/10.5194/amt-14-6119-2021, publisher: Copernicus GmbH, 2021.

Ruckstuhl, A. F., Henne, S., Reimann, S., Steinbacher, M., Vollmer, M. K., O'Doherty, S., Buchmann, B., and Hueglin, C.: Robust extraction of baseline signal of atmospheric trace species using local regression, Atmospheric Measurement Techniques, 5, 2613–2624, https://doi.org/10.5194/amt-5-2613-2012, publisher: Copernicus GmbH, 2012.

Saltzman, E. S., Savoie, D. L., Zika, R. G., and Prospero, J. M.: Methane sulfonic acid in the marine atmosphere, Journal of Geophysical Research: Oceans, 88, 10 897–10 902, https://doi.org/10.1029/JC088iC15p10897, _eprint: https://onlinelibrary.wiley.com/doi/pdf/10.1029/JC088iC15p10897, 1983.

Schmale, J., Sharma, S., Decesari, S., Pernov, J., Massling, A., Hansson, H.-C., von Salzen, K., Skov, H., Andrews, E., Quinn, P. K., Upchurch, L. M., Eleftheriadis, K., Traversi, R., Gilardoni, S., Mazzola, M., Laing, J., and Hopke, P.: Pan-Arctic seasonal cycles and long-term trends of aerosol properties from 10 observatories, Atmospheric Chemistry and Physics, 22, 3067–3096, https://doi.org/10.5194/acp-22-3067-2022, publisher: Copernicus GmbH, 2022.

Serreze, M. C. and Barry, R. G.: Processes and impacts of Arctic amplification: A research synthesis, Global and Planetary Change, 77, 85–96, https://doi.org/10.1016/j.gloplacha.2011.03.004, 2011.

Shao, L., Liu, P., Jones, T., Yang, S., Wang, W., Zhang, D., Li, Y., Yang, C.-X., Xing, J., Hou, C., Zhang, M., Feng, X., Li, W., and BéruBé, K.: A review of atmospheric individual particle analyses: Methodologies and applications in environmental research, Gondwana Research, 110, 347–369, https://doi.org/10.1016/j.gr.2022.01.007, 2022.

Si, M., Evoy, E., Yun, J., Xi, Y., Hanna, S. J., Chivulescu, A., Rawlings, K., Veber, D., Platt, A., Kunkel, D., Hoor, P., Sharma, S., Leaitch, W. R., and Bertram, A. K.: Concentrations, composition, and sources of ice-nucleating particles in the Canadian High Arctic during spring 2016, Atmospheric Chemistry and Physics, 19, 3007–3024, https://doi.org/10.5194/acp-19-3007-2019, publisher: Copernicus GmbH, 2019.

Siegel, K., Gramlich, Y., Haslett, S. L., Freitas, G., Krejci, R., Zieger, P., and Mohr, C.: Arctic observations of hydroperoxymethyl thioformate (HPMTF) – seasonal behavior and relationship to other oxidation products of dimethyl sulfide at the Zeppelin Observatory, Svalbard, Atmospheric Chemistry and Physics, 23, 7569–7587, https://doi.org/10.5194/acp-23-7569-2023, publisher: Copernicus GmbH, 2023.

Skamarock, W. C., Klemp, J. B., Dushia, J., Gill, D. O., Liu, Z., Berner, J., Wang, W., Powers, J. G., Duda, M. G., Barker, D. M., and Huang, X.: A Description of the Advanced Research WRF Version 4, https://doi.org/10.5065/1dfh-6p97, 2022.

Sprenger, M. and Wernli, H.: The LAGRANTO Lagrangian analysis tool – version 2.0, Geoscientific Model Development, 8, 2569–2586, https://doi.org/10.5194/gmd-8-2569-2015, publisher: Copernicus GmbH, 2015.

Stein, A. F., Draxler, R. R., Rolph, G. D., Stunder, B. J. B., Cohen, M. D., and Ngan, F.: NOAA's HYSPLIT Atmospheric Transport and Dispersion Modeling System, Bulletin of the American Meteorological Society, 96, 2059–2077, https://doi.org/10.1175/BAMS-D-14-00110.1, publisher: American Meteorological Society Section: Bulletin of the American Meteorological Society, 2015.

Stohl, A., Hittenberger, M., and Wotawa, G.: Validation of the lagrangian particle dispersion model FLEXPART against large-scale tracer experiment data, Atmospheric Environment, 32, 4245–4264, https://doi.org/10.1016/S1352-2310(98)00184-8, 1998.

Stohl, A., Eckhardt, S., Forster, C., James, P., Spichtinger, N., and Seibert, P.: A replacement for simple back trajectory calculations in the interpretation of atmospheric trace substance measurements, Atmospheric Environment, 36, 4635–4648, https://doi.org/10.1016/S1352-2310(02)00416-8, 2002.

Stohl, A., Seibert, P., Arduini, J., Eckhardt, S., Fraser, P., Greally, B. R., Lunder, C., Maione, M., Mühle, J., O'Doherty, S., Prinn, R. G., Reimann, S., Saito, T., Schmidbauer, N., Simmonds, P. G., Vollmer, M. K., Weiss, R. F., and Yokouchi, Y.: An analytical inversion method for determining regional and global emissions of greenhouse gases: Sensitivity studies and application to halocarbons, Atmospheric Chemistry and Physics, 9, 1597–1620, https://doi.org/10.5194/acp-9-1597-2009, publisher: Copernicus GmbH, 2009.

Storelvmo, T.: Aerosol Effects on Climate via Mixed-Phase and Ice Clouds, Annual Review of Earth and Planetary Sciences, 45, 199–222, https://doi.org/10.1146/annurev-earth-060115-012240, 2017.

Stuecker, M. F., Bitz, C. M., Armour, K. C., Proistosescu, C., Kang, S. M., Xie, S.-P., Kim, D., McGregor, S., Zhang, W., Zhao, S., Cai, W., Dong, Y., and Jin, F.-F.: Polar amplification dominated by local forcing and feedbacks, Nature Climate Change, 8, 1076–1081, https://doi.org/10.1038/s41558-018-0339-y, 2018.

Tewari, M., Chen, F., Wang, W., Dudhia, J., LeMone, M., Gayno, G., Wegiel, J., and Cuenca, R.: Implementation and verification of the unified Noah land surface model in the WRF model, 20th Conference on Weather Analysis and Forecasting/16th Conference on Numerical Weather Prediction, Seattle, WA, 2004.

Wen, D., Lin, J., Millet, D., Stein, A., and Draxler, R.: A backward-time stochastic Lagrangian air quality model, Atmospheric Environment, 54, 373–386, https://doi.org/10.1016/j.atmosenv.2012.02.042, 2012.

Wex, H., Huang, L., Zhang, W., Hung, H., Traversi, R., Becagli, S., Sheesley, R. J., Moffett, C. E., Barrett, T. E., Bossi, R., Skov, H., Hünerbein, A., Lubitz, J., Löffler, M., Linke, O., Hartmann, M., Herenz, P., and Stratmann, F.: Annual variability of ice-nucleating particle concentrations at different Arctic locations, Atmospheric Chemistry and Physics, 19, 5293–5311, https://doi.org/10.5194/acp-19-5293-2019, 2019.

Winiger, P., Andersson, A., Eckhardt, S., Stohl, A., and Gustafsson, : The sources of atmospheric black carbon at a European gateway to the Arctic, Nature Communications, 7, 12 776, https://doi.org/10.1038/ncomms12776, publisher: Nature Publishing Group, 2016.

Xu, J.-W., Martin, R. V., Morrow, A., Sharma, S., Huang, L., Leaitch, W. R., Burkart, J., Schulz, H., Zanatta, M., Willis, M. D., Henze, D. K., Lee, C. J., Herber, A. B., and Abbatt, J. P. D.: Source attribution of Arctic black carbon constrained by aircraft and surface measurements, Atmospheric Chemistry and Physics, 17, 11 971–11 989, https://doi.org/10.5194/acp-17-11971-2017, publisher: Copernicus GmbH, 2017.

Yun, J., Evoy, E., Worthy, S. E., Fraser, M., Veber, D., Platt, A., Rawlings, K., Sharma, S., Leaitch, W. R., and Bertram, A.: Ice nucleating particles in the Canadian High Arctic during the fall of 2018, Environmental Science: Atmospheres, 2, 279–290, https://doi.org/10.1039/D1EA00068C, publisher: RSC, 2022.

Zeng, Y. and Hopke, P. K.: A study of the sources of acid precipitation in Ontario, Canada, Atmospheric Environment (1967), 23, 1499–1509, https://doi.org/10.1016/0004-6981(89)90409-5, 1989.

Zhao, B., Donahue, N. M., Zhang, K., Mao, L., Shrivastava, M., Ma, P.-L., Shen, J., Wang, S., Sun, J., Gordon, H., Tang, S., Fast, J., Wang, M., Gao, Y., Yan, C., Singh, B., Li, Z., Huang, L., Lou, S., Lin, G., Wang, H., Jiang, J., Ding, A., Nie, W., Qi, X., Chi, X., and Wang, L.: Global variability in atmospheric new particle formation mechanisms, Nature, 631, 98–105, https://doi.org/10.1038/s41586-024-07547-1, publisher: Nature Publishing Group, 2024.